# HYBRID SUPERCAPACITORS BASED ON TWO DIMENSIONAL MATERIALS: MXENES, GRAPHENE AND TMDCS

Master Thesis

Ibrahim WONGE LISHESHAR

Eskişehir, 2019

# HYBRID SUPERCAPACITORS BASED ON TWO DIMENSIONAL MATERIALS: MXENES, GRAPHENE AND TMDCS

Ibrahim WONGE LISHESHAR

Master Thesis

Electrical & Electronic Engineering

Supervisor: Assoc Prof. Dr. Nihan KOSKU PERKGÖZ

Eskişehir

Eskişehir Technical University

Institute of Graduate Programs

December 2019

## FINAL THESIS APPROVAL

This thesis titled “Hybrid Supercapacitors Based on Two Dimensional Materials: MXenes, Graphene and TMDCs” has been prepared and submitted by Ibrahim WONGE LISHESHAR in partial fulfillment of the requirements in “Eskişehir Technical University Directive on Graduate Education and Examination” for the Degree of Master of Science (MSc) in Electrical and Electronics Engineering Department and has been examined and approved on December 27, 2019.

| Jury Members | Title & Name | Signature |
|---|---|---|
| Supervisor | Assoc Prof. Dr. Nihan KOSKU PERKGÖZ | …… |
| Member | Prof. Dr. Feridun AY | …… |
| Member | Dr. Faruk DİRİSAĞLIK | …… |

…….

Director,

Institute of Graduate Programs

# ÖZET

İKİ BOYUTLU MALZEME ÜZERİNE HİBRİT SÜPERKAPAKİTÖR: MXENLER, GRAFEN VE METAL KALKOJENİTLER

Ibrahim WONGE LISHESHAR
Elektrik ve Elektronik Mühendisliği Anabilim Dalı
Elektronik Bilim Dalı

Eşkişehir Teknik Üniversitesi, Lisansüstü Eğitim Enstitüsü, Aralık, 2019
Danışman: Doç Dr. Nihan KOSKU PERKGÖZ

Tüyler ürpertici küresel ısınmanın etkisiyle dünya, enerji üretimi alanında, daha çevre dostu yeşil enerji kaynakları için umut verici bir yönde değişiyor. Bu enerji sistemlerinin sürekli olmayan doğası, günlük enerji talebini karşılama yeteneklerini engellemektedir. Bu sorun için bir çözüm, piller ve süper kapasitörler (SK'ler) gibi enerji depolama sistemlerinin geliştirilmesinde bulunmaktadır. Yüksek güç yoğunluğuna sahip olmalarına rağmen, SK'ler genellikle düşük enerji yoğunluğu muzdariptir. İstenen verimli yük depolama kapasitesine sahip elektrot malzemelerinin tasarımı, alınan çok sayıda yoldan biridir ve iki boyutlu (2B) malzemelerin kendine özgü elektrokimyasal özelliklere sahip olması, elektrot malzemeleri uygulamasında araştırmalarını motive etmiştir. Bir veya birkaç katta görünüşte abartılı performans göstermesine rağmen, 2B malzemeler yığılmadan muzdarip olma eğilimindedir ve bu kapasitif potansiyellerini önemli ölçüde azaltır. Bu çalışma, SK uygulaması için 2B materyallerin (Grafen, Geçiş Metal Kalkojenitleri, MXenler) büyütülmesine yöneliktir. ~ 0.63 nm kalınlığında grafen ile yapılan SK'ler, 1M $Na_2SO_4$ elektrolitte 1 mV $s^{-1}$ oranında 44 uF $cm^{-2}$ özgül kapasitans ve 308 F $g^{-1}$ gravimetrik kapasitans performansı gösterirken bunu üst üste yığılan sekiz kat grafen ile 154 μF $cm^{-2}$'ye yükselmiştir. En yüksek gravimetrik kapasitans, 1.26 nm kalınlığındaki grafen için, 1 mV $s^{-1}$'de 441 F $g^{-1}$ olacak şekilde, 12.4 kW $g^{-1}$ güç yoğunluğunda 39.2 Wh $kg^{-1}$ enerji yoğunluğu ile ölçülmüştür. Sonlandırılmamış MXenler süper iletkendir ve iyon araya ekleme için büyük ara katman aralığına sahiptir. Kimyasal buhar biriktirme yöntemi ile büyütülen $Mo_2C$, 1 mV $s^{-1}$ tarama hızında ~ 671 uF $cm^{-2}$'lik bir kapasitans kaydederek oldukça ilginç sonuçlar göstermiştir.

**Anahtar Kelimeler:** Süper kapasitör, özgül kapasitans, CVD ve MXen.

## ABSTRACT

HYBRID SUPERCAPACITORS BASED ON TWO DIMENSIONAL MATERIALS: MXENES, GRAPHENE AND TMDCS

Ibrahim WONGE LISHESHAR

Department of Electrical & Electronics Engineering

Electronics Specialization

Eskişehir Technical University, Institute of Graduate Programs, December, 2019

Supervisor: Assoc Prof. Dr. Nihan KOSKU PERKGÖZ

Stroke by the dreadful global warming, the world is changing in the field of energy generation in a direction auspicious for more environment friendly green energy sources. The interruptible nature of these energy systems hinders their ability to meet the over everyday energy demand. A remedy to this is found in the development of energy storage systems such as batteries and supercapacitors (SCs). Albeit endowment with high power density, SCs most often suffer from low energy storage capabilities. The design of electrode materials with desired efficient charge storage capabilities is one of the multiple pathways taken to boast device performance, and the discovery of 2D materials with peculiar electrochemical properties has nonetheless motivated their research as electrode materials. Although seemingly overrated performance at one or few layers, 2D materials tend to suffer from agglomeration, markedly reducing their capacitance. This study is directed at the growth of 2D materials (Graphene, Transition metal dichalcogenides; TMDCs and MXenes) and their SC application. SCs constructed with ~0.63 nm thick graphene measured a specific capacitance of 44 μF $cm^{-2}$ and an gravimetric capacitance of 308 F $g^{-1}$ at a rate of 1 mV $s^{-1}$ in 1M $Na_2SO_4$ electrolyte, which increased to 154 μF $cm^{-2}$ at 8 times the initial thickness, suggesting little restacking. The highest gravimetric capacitance was measured for the 1.26 nm thick graphene to be 441 F $g^{-1}$ at 1 mV $s^{-1}$ with an energy density of 39.2 Wh $kg^{-1}$ at a power density of 12.4 kW $g^{-1}$. Non-terminated MXenes are superconductive and possess large interlayer spacing for ion intercalation. $Mo_2C$, as grown by CVD, demonstrated rather interesting results, recording a capacitance of ~671 μF $cm^{-2}$ at a scan rate of 1 mV $s^{-1}$.



**Keywords:** Supercapacitor, Specific Capacitance, CVD and MXenes.

## ACKNOWLEDGEMENTS

First and foremost, I would like to express my sincerest gratitude to the Turkish Government Scholarship (Yurtdışı Türkler ve Akrabalar Topluluklar Başkanlığı, YTB) for financing this program up to the very end.

Having been a member of the Micro Nano Systems and Devices Research Group (MIDAS), I would like to express my sincere gratitude to my supervisors: Assoc. Prof. Dr. Nihan KOSKU PERKGÖZ and Prof. Dr. Feridun AY for their academic as well as emotional support throughout my master program. Their deep experience, quick insight and keen observation, expert experimental and theoretical skills greatly inspired me. Their patient guidance and witty counseling have contributed immensely to my personal as well as academic growth. It has been a fortune and a great honor to have worked with them and I will forever be thankful.

My endearing gratitude goes to all the members of the MIDAS family. With their continues support and cooperation, they provided an environment without which successful completion of this work would have been a cumbersome hurdle. I would like to specifically thank Hüseyin Şar for his orientation and continuous support in technical aspects of this study, Merve Öper- 'the mother of MXenes, a friend whose hard work inspired me and Yahya Shehu.

Ibrahim WONGE LISHESHAR

27.12.2019

**STATEMENT OF COMPLIANCE WITH ETHICAL PRINCIPLES AND RULES**

I hereby declare in earnest that this thesis is an original work prepared by me; that I have conducted myself in accordance with scientific ethical principles throughout the stages of preparation, data collection, analysis and presentation of my work; that I have cited the sources of all the data and information that could be obtained within the scope of this study, and included these sources in the reference section; and that this study has been scanned for plagiarism with "scientific plagiarism detection program" used by Eskişehir Technical University, and that "it is free from any plagiarism" whatsoever. I also declare that, if a case contrary to my declaration is detected in this work at any time, I hereby express my consent to all the ethical and legal consequences that might be involved.

Ibrahim WONGE LISHESHAR

**TABLE OF CONTENTS**

## LIST OF FIGURES

**Page**

## GLOSSARY OF SYMBOLS AND ABBREVIATIONS

| | |
|---|---|
| AC | Activated Carbon |
| ac | Alternating Current |
| AFM | Atomic Force Microscopy |
| AN | Acetonitrile |
| CCCD | Constant Current Charge Discharge |
| CNT | Carbon Nanotube |
| CV | Cyclic Voltammetry |
| CVD | Chemical Vapor Deposition |
| DIC | Differential Interference Contrast |
| DI water | Deionized water |
| EDLC | Electrochemical Double Layer Capacitor |
| EIS | Electrochemical Impedance Spectroscopy |
| ESR | Equivalent Series Resistance |
| FWHM | Full Width Half Maximum |
| HF | Hydrofluoric acid |
| IPA | Isopropanol |
| MFC | Mass Flow Controller |
| MSC | Micro Supercapacitor |
| MXene | Transition Metal Carbide/ Nitride or Carbonitride |
| PDF | Partial Differential Equation |
| PECVD | Plasma Enhanced Chemical Vapor Deposition |
| PET | Polyethylene Terephthalate |
| PVA | Polyvinyl Alcohol |
| RGO | Reduced Graphene Oxide |
| SC | Supercapacitor |
| SCCM | Standard Cubic Centimeters per Minute |
| TMDC | Transition Metal Dichalcogenide |
| TMH/TMO | Transition Metal Hydroxide or Oxides |

# 1. INTRODUCTION

Man has come a long way since the discovery of energy, which has then become the main driving force behind technological breakthroughs. Uninterrupted supply of this power source is now a basic requirement. Many sources (hydro, fossil fuel, hydrothermal, nuclear, solar, wind etc.) are available to produce electrical energy which can then be converted easily into other forms of energy. Energy sources like nuclear, and fossil fuel are toxic to the environment demanding the exploration of alternative renewable environmentally friendly sources like solar, wind and hydro. However, most of these energy sources are seasonal and cannot provide incessant supply of the required energy. More so, energy demand is not constant in the course of the day, or even throughout the year. Energy storage systems offer a solution to this issue and those commonly used are batteries, supercapacitors and fuel cells. Like batteries and fuel cells, supercapacitors are energy storage devices, but with the ability to deliver this energy at extremely high speed. They can undergo thousands to tens of thousands of charge/discharge cycles with little or no degradation.

## 1.1. Thesis Organization

In this dissertation, the growth and characterization of 2D materials is discussed followed by their supercapacitor applications. The second chapter gives a general overview of supercapacitors which starts with the historical journey of the supercapacitor in section 2.1, followed by a summary of energy storage technologies. Section 2.3 highlights the salient features of the supercapacitor such as energy storage mechanism. Section 2.3.1 describes emulation models of supercapacitors. A comparative analysis of supercapacitors and other energy storage systems is discussed in section 2.3.4 after which some applications of supercapacitor are discussed. Research in supercapacitor has taken different forms and this is elucidated in the next section 2.3.6. Section 2.3.7 outlines some challenges faced by SC and possible ways to remedy them. The chapter concludes by with original contributions and motivation of the dissertation.

Chapter 2 targets the synthesis of 2D materials and their characterization. In the beginning of the chapter, reasons for choice of CVD technique are highlighted. Section 3.1 describes the synthesis of graphene and its characterization. Section 3.2 explores the growth of TMDCs starting with $MoS_2$ and then $MoSe_2$ as well as material characterization. The

following section discusses the synthesis of $Mo_2C$ and finally in section 3.3.1 the material properties are examined by Raman and AFM techniques.

The last chapter of this thesis discusses the fabrication of SCs using different 2D materials. The chapter opens by shading light on the reasons for research attention in 2D materials. Section 4.1 examines the performance of Sc fabricated using different stacks of graphene layers. It encompasses the device fabrication procedures as well as characterization and discussion of obtained results. Section 4.2 evaluates the performance of the MXene, Graphene hybrid SC. Section 4.2.3 discusses the various approaches that can be taken to enhance the performance of the fabricated devices. Section 4.4 highlights the benefits of using TMDCs for supercapacitor application. The final section of this dissertation, section 4.4 gives an analysis of the results obtained in this work with comparing them to previous studies in literature.

# 2. OVERVIEW AND LITERATURE REVIEW

## 2.1. A Brief History

The concept of static electricity was known in the ancient times as was evident with the rubbing of ambers, the origin of which could only be understood until 140 years later when light began to shed on molecular level electricity. The discovery of the electron in 1897 by J.J Thomson and the invention of the three electrode valve in 1906 swelled the popularity of electronics [1]. The invention of the Leyden jar in 1745 by the German Von Kleist et al. and independently by Pierre van Musschenbroek in the Dutch city of Leyden [2, 3], marked the first significant step towards energy storage. This was a simple device made up of a glass vial, wrapped in a metallic foil. The phial was partially filled with water, the orifice of which was corked, with a nail dipped into the water via the seal (see Figure 2.1). A later version by Benjamin Franklin, known as the dissectible capacitor, made use of a sheet of glass sandwich in two foil electrodes [4, 5]. Michael Faraday was the pioneer inventor of the fixed and variable capacitor, as well as introducing the concept of the dielectric constant. The unit of capacitance was named after him, due to his major contribution in this field. Later improvements of capacitors utilized rigid metal electrodes and air, vacuum, mica or polystyrene dielectrics.

**Figure 2.1.** *The leyden jar (Bakken museum)*

The earliest capacitor used in radio receivers as power filters or in RF circuits was invented by Fitzgerald in 1876 [3, 6] and made use of foil electrodes and wax-impregnated paper dielectrics. In 1909, mica capacitors were invented which were more reliable as mica is an excellent dielectric material, with an outstanding discharge resistance [3]. Work on electrolytic capacitors dates back to 1897 when Charles Pollak patented a borax electrolytic capacitor with Aluminum electrodes. Electrolytic capacitors did not become popular and more reliable until after World War II, when more research attention was given to ameliorate earlier shortcomings [7]. Ceramics, porcelain, steatite, cordierite, and rutile were among the dielectric media in use until the discovery of Barium Titanate in 1941 [3] with a dielectric in the scale of 1000. This caused a shift in research attention towards the Barium Titanate family of materials.

Mansbridge patented a metalized, self-clearing paper capacitor in 1900 [3, 8]. Metalizing with metal particle-filled binders resulted in frequent shorts through the paper. This was later mitigated by employing vacuum deposited metal and lacquer coated paper, with the benefit of reduced metal corrosion by electrolyte as well as improved insulation resistance [9]. Polyethylene terephthalate (PET) was introduced into the capacitor world in 1941 and saw so many changes. In 1959 [10] capacitors with dielectrics made from polyethylene, polystyrene, polytetrafluoroethylene, PET, and polycarbonate were manufactured. Around the 1970's, film-foil capacitors, without paper, were being deployed for applications such as electric utility [3].

The use of porous carbon in electrodes was investigated as far as the 1950's. The capacitor architectures were inspired by those of rechargeable batteries and fuel cell. The very first supercapacitor was invented and patented by H. Becker in 1957 [11]. This device was characterized by light weight, compactness, low voltage and high capacitance. It made use of porous carbon or sticks of fired tar lampblack electrodes, Pyrex glass wool separator and a rubber gasket in-between the electrodes and the separator and a salt ($NH_4Cl$) or acidic electrolyte (aqueous $H_2SO_4$).

Another version of Becker's invention,- "The electrical energy storage apparatus"-, was demonstrated in 1966 using porous graphite electrodes [12]. The amount of energy stored in this apparatus could be enhanced by introducing activating chemical reagents

capable of redox activity at the electrode – electrolyte interface thus, laying the foundation for pseudo-capacitors.

The differences between a supercapacitor and a battery were alienated in 1991 by B. E. Conway [13] who had attributed so much research effort in this field. Earlier supercapacitors had high internal resistance, limiting discharge current. Supercapacitors that can store high energy and still be able to maintain durability and high charge and discharge rates are still a far cry from realization. However, research on supercapacitors continue to mature as more technology is discovered. The main research focus in on potential electrode materials, electrolytes, device architecture and methods to increase charge storage capability.

## 2.2. Energy Storage Systems

Energy storage systems provide a wide array of technological approaches to managing our power supply. The aim here is to create a more resilient energy infrastructure and bring cost savings to utilities and consumers. The methods and technology used to store various forms of energy is known as energy systems. There are a myriad different types of energy storage technologies which can be characterized into 7 different storage systems [14, 15].

i. **Electrochemical.** Here, energy storage involves a conversion of chemical energy to electrical energy. Examples under this family are batteries- ranging from lead-acid batteries to Lithium polymer batteries.

ii. **Electrostatic.** Energy is stored in an electrostatic charge separation, or by both electrostatic and chemical redox conversions. Examples are capacitors, super/ultra-capacitors.

iii. **Electromagnetic.** An example here is the superconducting magnetic energy storage system. It stores energy in a magnetic field, when direct current is passed through a coil of cryogenically cooled superconductor.

iv. **Chemical.** Like batteries, energy is stored in chemical bonds but unlike batteries it is produced from an external fuel supply. Examples include hydrogen and fuel cell storage systems.

v. **Kinetic.** Flywheels are an example of kinetic energy storage technology. The momentum in a rotating mass is captured, and then applying a torque to a mechanical load.

vi. **Potential.** Energy is stored by introducing a potential difference. This can then be utilized to turn a turbine, generating electricity. Examples are cryogenic and pumped hydropower storage systems.

vii. **Thermal**. Just as the name suggests, energy is stored as a form of heat and can then be converted into electricity. Belonging to this family are, molten salt batteries, solar ponds and heat pumps.

### 2.2.1. Capacitors

A capacitor is an electronic device capable of storing, filtering and regulating electrical power. A capacitor stores energy in an electric field of two electrodes that sandwich an insulating layer called the dielectric layer.

A simple construction of a supercapacitor constitutes two metal plates held apart by a dielectric medium (Figure 2.2). Dielectrics can be insulators such as vacuum (dielectric constant, $\varepsilon_r = 1$), air ($\varepsilon_r = 1.0006$), Ceramic ($\varepsilon_r = 30 - 7500$), Mica ($\varepsilon_r = 5.5$), Mylar ($\varepsilon_r = 3$), Oil ($\varepsilon_r = 4$), dry Paper ($\varepsilon_r = 2.2$), Polystyrene ($\varepsilon_r = 2.6$) and Teflon ($\varepsilon_r = 2.1$) [16]. The measure of how much charge can be stored by the plates of a capacitor for a given amount of applied potential difference is called capacitance, measured in Farads– named after Michael Faraday due to his significant work in this field. Capacitors find applications as decouples, where they enable sudden transfer of energy while maintaining a constant voltage, as filters removing or reducing unwanted ac signals as in AM radios and cellular telephones. They are also employed in smart meters as couplers to block dc signals while passing ac in smart meters. Capacitors are also used in timing and wave shaping to set delay time in windshield wipers [17].

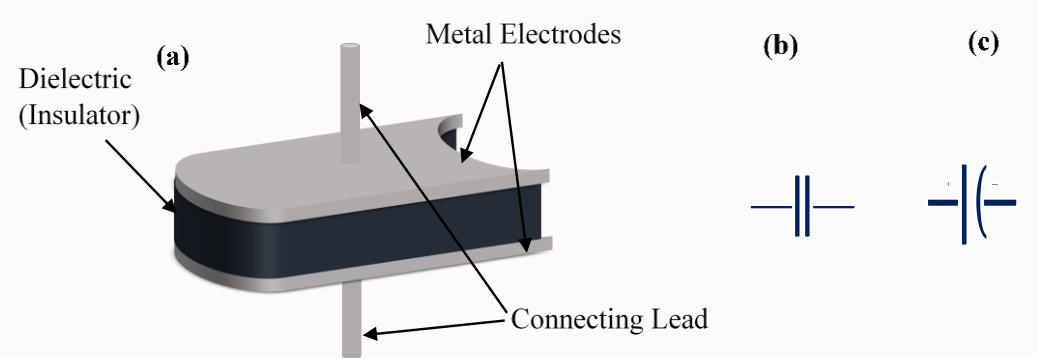


**Figure 2.2.** *Sandwich Capacitor: (a) parallel Plate Capacitor, (b) Schematic Symbol and (c) Symbol of polarized capacitor*

#### *2.2.1.1.Factors affecting the performance of a capacitor*

The performance of a capacitor can be measured by the phase difference of its alternating current and voltage, the amount of leakage current and capacitance stability. An ideal capacitor has zero leakage current, does not dissipate energy and maintains the desired constant capacitance over time. However, there is no ideal capacitor and several factors causes a capacitor to deviate from idealness.

***Capacitance***

As mentioned before, the measure of how much electrical charge a capacitor can store for a given applied potential is called its capacitance and is measured in SI units of Farads. 1F is defined as one coulomb of charge stored for one volt of applied potential difference. A typical capacitor measures in the range of picofarads to millifarads [18]. Capacitance of a capacitor increases linearly as the permittivity of the dielectric and the surface area of the electrode plates and decreases as the distance between the separators increases as shown in E.2.1.

$$C = \frac{Q}{V} = \frac{\varepsilon A}{d} \tag{2.1}$$

C is the capacitance, Q, the total charge accumulated on the two plates, V, the voltage across the plates, ε the dielectric constant, A the total surface area of the electrode available for charge storage and d, is the distance between the two electrodes.

***Leakage current and insulation resistance***

When a capacitor is fully charged, depending on the insulative capability of the dielectric, a small DC current can slowly leak through the dielectric, slowly discharging the capacitor. This is called self-discharge and leads to a drop in the charged voltage in the course of time. The insulation resistance is the resistance offered by the dielectric to flow of the leakage current. This is expressed mathematically in E.2.2., where $I_{lk}$ is the leakage current and $R_{ir}$, is the insulation resistance.

$$I_{lk} = \frac{V}{R_{ir}} \tag{2.2}$$

The terms leakage current and insulation resistance are used interchangeably depending on the size of the leakage current. If the leakage current is very high then leakage

current becomes the pertinent term (e.g. Al electrolytic capacitors), otherwise insulation resistance is used (e.g. in ceramic capacitors) [17].

Insulation resistance is lower for high capacitance capacitors whereas, the leakage current is temperature dependent and increases as temperature rises.

***Dielectric breakdown voltage***

The energy that can be stored in a capacitor is proportional to the square of the applied potential. However, if this is so high, the force on the electrons becomes so great that it literally forces them out of their orbits [16]. The areas where breakdown occur might become permanently conductive due to several compounds such as carbon formed during the breakdown. The capacitor becomes a short-circuit or an insulation resistance reject [17].

***Equivalent series resistance***

A purely ideal capacitor is characterized by having an impedance, where the real and imaginary components are out of phase by 90 ° at periodic changes in current and/or voltage and independent of frequency when a sinusoidal alternating voltage is applied. The phase difference in impedance components of a real capacitor usually runs short of 90 ° and varies with frequency, indicating the presence of a resistive and an inductive component. The impedance of a real capacitor is usually embodied by a purely capacitive component in series with an ohmic component otherwise known as the equivalent series resistance (ESR) [1]. Generally, ESR arises from the resistance of the metal (current collector)- electrode interface, the electrode (active material for supercapacitors), the connection lead contact and the electrolyte or the dielectric loss [19].

A simple model of a capacitor comprises of an ohmic component connected in series with a purely capacitive component as shown in Figure 2.3. This representation has a frequency dependent impedance $Z(\omega)$ given in E.2.3. As the frequency approaches infinity, this impendence tends to ESR, thus providing a formal means for estimating the value of ESR. In a Nyquist plot, the ESR is evaluated as the intercept on the imaginary axis as $\omega \rightarrow \infty$ [1].

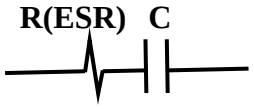


**Figure 2.3.** *A simple circuit representation of a capacitor.*

$$Z(\omega) = ESR + \frac{1}{j\omega C} \tag{2.3}$$

***Post charge/ discharge relaxation voltage***

EDLCs after having been charged or discharged, tend to experience a drift in voltage, relaxing towards its previous level as time goes by. This voltage relaxation is likely due to long diffusion time of the porous electrodes of an EDLC and occurs over extended durations (hours). Voltage relaxation can manifest in both directions– charged or discharged – and can be influenced by the amount and duration of the applied current as well as the voltage [20].

***2.2.1.2.Energy storage mechanism in capacitors***

Capacitors store charge in an electric field established by opposing charges collecting on the two electrodes. Before a potential difference is applied between the capacitor plates, the number of electrons in each plate is the same. Upon dc voltage application, electrons are removed from one of the plates (anode) and an equal number are deposited on the other (cathode). As a result of excess charges, the cathode becomes negatively charged relative to the anode, thus creating an electrostatic field between the plates [21]. This electric field is maintained by the help of the dielectric which prevents the capacitor from self-discharge. The energy stored by a capacitor is directly proportional to its capacitance and to the square of the applied voltage as shown in E.2.4, where C stands for capacitance and V the applied voltage.

$$E = \frac{1}{2} CV^2 \tag{2.4}$$

## 2.3. Supercapacitors

A super/ultra-capacitor in principle is a capacitor with high energy storage capability. They are usually characterized by their high capacitances which is made feasible by the use of high surface area electrode materials and thin electrolytic dielectrics [1, 22, 23]. Basically, a simple super capacitor cell is constructed from two electrodes and an electrolyte impregnated thin porous separator placed in the embrace of the two electrodes as shown in Figure 2.4. The electrode usually constitutes a high specific areal material (the active material) such as activated carbon [24] plastered onto a metal current collector with the help of binders. It is worth mentioning that an electrode material should be chemically and

electrically compatible with the electrolyte used, since we do not want the electrolyte to react with the active material.

The function of the separator is to act as a membrane, keeping the electrodes from electrical contact, while allowing mobility of charged electrolyte ions. The thickness of the separator, porosity, electrical and mechanical properties must contribute to effect efficient isolation of the tightly pressed electrodes as well as ensuring high conductivity of electrolyte ions via its pores. It must be chemically inert to electrolyte and the electrodes and must not introduce undesirable additives like humidity, gases and air [25]. Separator materials are generally cellulose (paper), fiberglass textiles, polymers. Cellulose based separators, e.g. acetonitrile (AN) [26] and polypropylene [25] are more suitable for electrolytes that are organic in nature due to their better wettability in these electrolytic media but depreciate rapidly in aqueous electrolytes [27, 28]. For aqueous electrolytes ($H_2SO_4$, KOH, etc.), fiberglass separators (e.g. plasma modified polymer nonwoven fabrics such as polyamide [25]) exhibit better performance [29, 30]. Propylene and ethylene carbonates effect lower equivalent series resistance and increased capacitance when ionic liquid electrolytes (e.g. Li based electrolytes) are used as they can absorb the electrolyte very well [31].

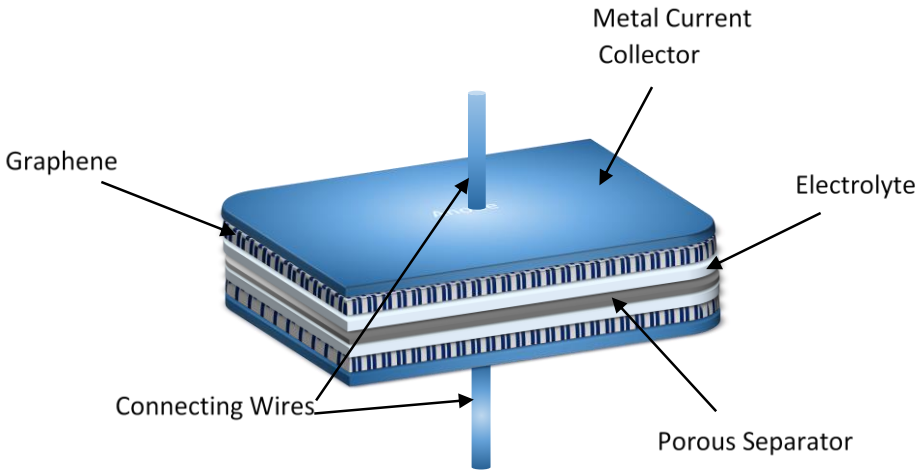


**Figure 2.4.** *A simple structure of double layer supercapacitor*

### 2.3.1. Charge storage mechanism

Charge storage in supercapacitors is achieved mainly through charge separations. There are several models explaining how this is done. Based on the energy storage

mechanism, supercapacitors can be characterized into electrochemical double layer (EDLC), pseudo capacitors and hybrid capacitors [32] as shown in Figure 2.5.

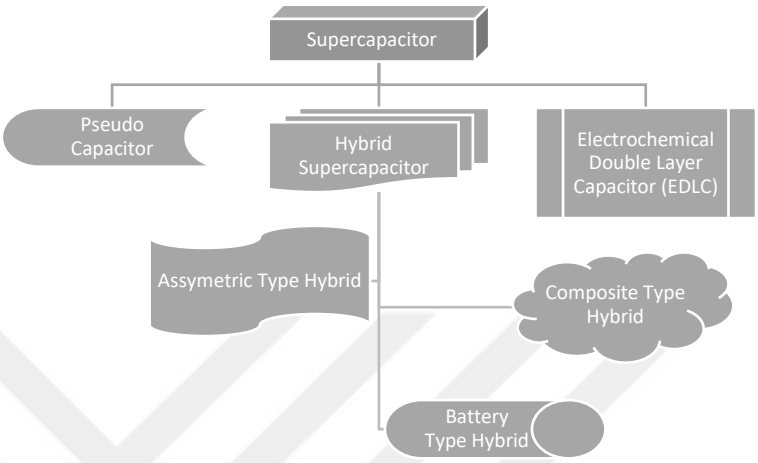


**Figure 2.5.** *Taxonomy of supercapacitors (adapted from Halper, 2006)*

### *2.3.1.1.Electrochemical double layer capacitor (EDLC)*

As the name suggests, an electrochemical double layer capacitor is built up of two electrodes, sandwiching and electrolytic medium and kept from electrical contact by a porous separator. Charge in an EDLC is stored at the electrode electrolyte interface by non-faradic (electrostatic) means, without allowing charge transfer between electrode and electrolyte except via unavoidable leakage. EDLCs generally operate with stable capacitance for many charge-discharge cycles, sometimes as many as $10^6$ cycles [32]. Most EDLCs use carbon base materials due to their high surface area [33].

***Properties of EDLCs***

The electrostatic charge storage mechanism of EDLCs endow them with high power density. This off course also depends on the conductivity of both the electrode material and type of electrolyte used. EDLCs usually have a high life span. They can undergo tens of thousands of charge-discharge cycles, losing little or none of their original capacitance. Thus, EDLCs are characterized by high speed (power density), and durability. However, they can only store a small amount of energy, which is directly proportional to the capacitance which in turn is proportional to the surface area (active area in the pores where the double layer is

formed) and the electrolyte ion to electrode pore size ratio [22]. Specific capacitance is the value of the capacitances normalized by mass (E.2.5).

$$C_{sp} = \frac{Capacitance\ (F)}{Mass\ (g)} = \left(\frac{F}{cm^2}\right)_{act} * \left(\frac{cm^2}{g}\right)_{act} = volumetric\ Capacitance * density \quad (2.5)$$

The equation of the active volumetric capacitance can also be written as

$$C_v = \left(\frac{F}{cm^2}\right)_{act} = \left(\frac{k}{t}\right)_{eff} \quad (2.6)$$

Where, t is the thickness of the double layer, and k is the dielectric constant. Calculating the effective dielectric constant and the thickness of the double layer formed at the electrode electrolyte interface is complicated and not well understood [1]. However, the thickness of the double layer is usually in the nanometer scale making for high specific capacitances in the range of 15 to 30 $\mu F cm^{-2}$. This is equivalent to a specific capacitance of 150 F $g^{-1}$ to 300 F $g^{-1}$ for an active area of 1000 $m^2$ $g^{-1}$. Unfortunately, the specific capacitance of carbon electrodes is usually lower, in the range of 75 to 170 F $g^{-1}$ and 40 to 100 F $g^{-1}$ in aqueous and organic electrolytes respectively. This is accounted by the fact that a large area of the electrode is inaccessible by electrolyte ions, due to ions being larger than the pores [22]. Therefore, in designing a supercapacitor, the ratio of pore size to the ion size should be taken into careful consideration, as large ions entail low capacitances and very small pores dictates greater decrease in capacitance as the scan rate increases.

The durability of EDLCs make them well suited for applications in locations where user access is difficult or impossible, such as deep seas, mountain environments, thick forests and space [23].

***2.3.1.2.Pseudo capacitors***

A pseudo capacitor like an EDLC, is built in the same way; however, it differs in its charge storage mechanism. Energy is stored through three processes: electrostatically like in EDLCs, via fast faradic reactions between the electrolyte and the electrodes and through doping and un-doping of active electrode material. Thus, the interaction at the electrode electrolyte interface involves breaking and rebuilding of chemical bonds in voltage-dependent (C = dQ/dV) redox reactions which are best referred to as charge transfer reactions. Ion adsorption and redox reactions are surface dependent reactions and therefore

depend on the surface area of the electrodes, whereas doping and un-doping are bulk processes. In order to obtain high specific pseudo capacitances, high electron conductive and large surface area electrodes material with the right pore size are needed for the distribution of ions and current collection [1, 22, 34]. The synergy of multiple charge storage processes results in pseudo capacitors that have higher specific capacitances as compared to EDLCs and thus a corresponding higher energy density. Examples of pseudo active materials include Metal Oxides/ or hydroxides e.g. $RuO_2$ [35] and doped conducting polymers [36].

***2.3.1.3.Hybrid supercapacitors***

EDLCs have high power density and can undergo longer charge discharge cycles, while pseudo capacitors can store more energy but are relatively less durable. By attempting to bridge the gap between EDLCs and pseudo capacitors, hybrid capacitors aim to synergize their individual advantages while alleviating their shortcomings. By employing both faradic and non-faradic charge storage mechanisms, hybrid supercapacitors can store more energy than EDLCs, exercise higher power density than pseudo capacitors while maintaining a good cycling stability and affordability [32]. Three types of hybrid supercapacitors are distinguishable by their electrode configuration as illustrated in Figure 2.5 – i.e. asymmetric type, composite and battery type hybrid.

***Asymmetric type hybrid supercapacitor***

Configured with one electrode of an EDLC and the other of a pseudo active material, an asymmetric hybrid capacitor can accumulate charge via faradic reactions (and/or doping and un-doping) as well as electrostatically. This does not only increase the specific capacitance but also widens the voltage window of the device. Most asymmetric supercapacitors preferably couple a pseudo capacitor material as the cathode due to the difficulty– e.g. high resistance encountered in n-doping- in obtaining an efficient negative charged pseudo active material as prevalent in conductive polymers [32, 37]. And EDLC material offers the benefit of cycle stability and low equivalent series resistance, thus improving the overall power density. An example is a hybrid configuration with 90% activated carbon as cathode and an 80% p-doped poly(3-methylthiophene) anode [38, 39].

***Composite type hybrid supercapacitor***

This describes a type of supercapacitor where the electrode's active material is an amalgam of two or more different materials, integrating both physical and chemical charge storage processes in a single electrode, aiming to achieve mutual cancellation of the individual material's shortcomings. A composite supercapacitor can be constructed with an EDLC material with the advantage of fast charging and discharging and high conductivity, and a pseudo active material with the benefit of high surface area for redox activity [32]. A carbon nanotube/ polymer (e.g. polyaniline or polypyrrole) [40, 41] demonstrates improved electrical, mechanical and electrochemical properties compared to polymers alone.

***Battery type hybrid supercapacitor***

Batteries can store more energy than supercapacitors, so if one of a supercapacitor's electrode is replaced by a battery electrode, a supercapacitor can be expected to gain a boost in energy density. This is a special type of an asymmetric hybrid supercapacitor. Research in this field suggests that battery type hybrids can bridge the energy gap between supercapacitors and batteries by combining the higher energy density of batteries and specific power, short charge time, cycle life as well as reversibility of supercapacitors [42]. A battery type hybrid can be an EDLC electrode coupled with a battery type electrode. An example is using a high voltage intercalation compound $LiNi_{0.5}Mn_{1.5}O_4$ as the positive electrode in combination with an activated carbon negative electrode in a hybrid configuration [43], obtaining a capacity of 25 mAh $g^{-1}$ with an 80% retention after 1000 cycles. It could also be constructed with a pseudo active and a battery electrode [42]. A typical example is built with $Ti_2C$– MXene nanosheet anode and alluaudite $Na_2Fe_2(SO4)_3$ cathode, using an organic electrolyte, achieving a high specific energy of 260 Wh $kg^{-1}$ [44].

### 2.3.2. Supercapacitor models

An enabling management system is of paramount importance for error-free, handy and secure operability of SCs [45]. It manages thermal and cell equalization, power control synthesis and safety supervision of an SC, all hinging on control engineering [46]. Precise and efficient state estimation furnishes information on cell uniformity suppression and optimal power control of SC systems. In this vein a lucid understanding of the state of health**,** electrochemical, thermal and electrical behavior of an SC, is an unavoidable prerequisite. SC

models, via analysis and simulation, examine and forecast varied SC behaviors, thus eliminating efforts and costs in unnecessary practical experimentation. Algorithms that ensure system safety and reliability require efficient SC models. Accurate models eliminate the desire for overly control as well as boosts the operation range, thus enhancing system performance and efficiency [47]. Additionally, self-discharge, an obscurity in practical applications, in the form of charge redistribution mechanisms is dealt with a priori. SC models are a valuable tool for design prediction, condition monitoring and control synthesis [48].

An SC model is a surrogate on which prototype systems can then be designed, and its accuracy is determined by the assumptions made and the parameters considered, therefore designed to serve specific purposes. In this way, a raft of models has been reported in literature which can be classified based on the purpose they served, such as to emulate the electrical behavior, device heating, state of health, charge-discharge and charge storage.

The electrical behavior of an SC is most commonly emulated in electrochemical models, equivalent circuit models, and fractional-order models. It is worth mentioning that, there is a tradeoff for simplicity– ease of parameter identification efficiency- and accuracy, to be considered for each model. For example, electrochemical models are generally more accurate however troubled by low calculation efficiency. This is because they employ partial differential equations (PDEs) to capture the real internal reactions occurring inside an SC, however parameterization of PDFs requires arduous calculations. This stems their deployment in embedded systems for real-time energy management and control. On the other hand, equivalent circuit models are derived from empirical experience and experimental data under predetermined conditions. Under varying conditions, equivalent circuit models are rendered useless as model mismatch issues thwart their accuracy. In addition, their parameters and states lack physical representations so that no internal information is explicitly available. However, their structural simplicity and a decent modeling accuracy make them acceptable for real-time energy management [48].

Another modeling strategy is the so called intelligent or smart model. Smart models solicit biologically inspired neural networks and benefit from real-time adaptive machine learning to mimic SCs with accuracy. Physics based reduced-order models are meant to imitate an SC's voltage and internal parameters with speed and accuracy. Information from

these internal variable can be used to predict premature degradation of precursors hence can be used by controls in an EDLC management system to protect the device [47].

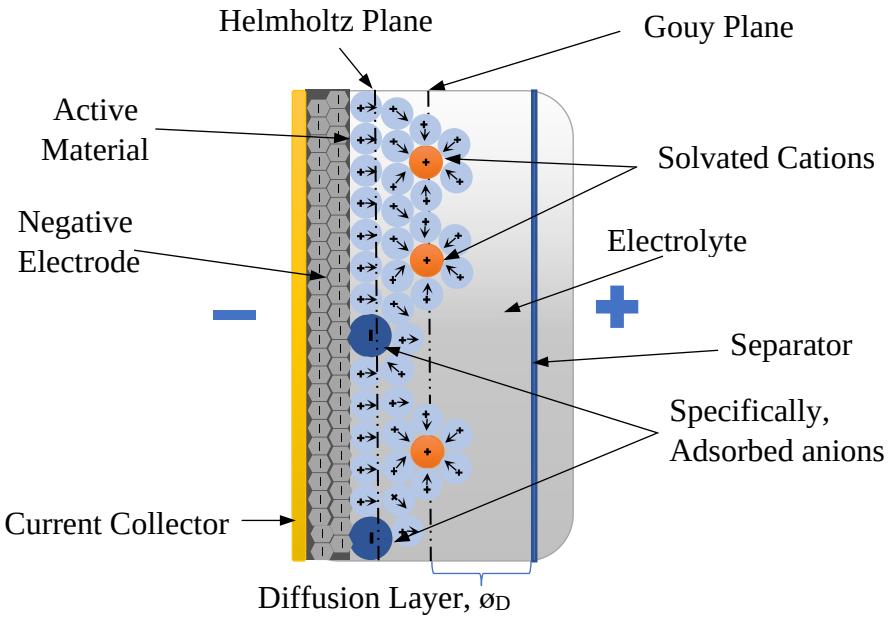


**Figure 2.6.** *A model of the supercapacitor double layer (adapted from Bockris, 1963)*

### *2.3.2.1.Electrochemical models*

An EDLC stores energy as charge in micropores of the active material, at the double layer formed when the solid electrode surface and liquid electrolyte interact. An explanation of the double layer of an EDLC has been proposed by so many models, an example of which is the Grahame model. It described three distinguishable regions: the inner Helmholtz layer, the outer Helmholtz layer and a diffuse ion distribution region [1, 49]. A more elaborate model was proposed by Bockris, et al [50] as shown in Figure 2.6. An electrolyte is made up of salt (solute) ions dissolved in a solvent. When a potential difference is applied to the electrodes; the solvent becomes polarized. Polarized solvent molecules with charge opposite that of the electrode, adhere electrostatically to the electrode forming a one molecular thick layer called the Inner Helmholtz layer. Ions with radius higher than 1.4 Å get specifically adsorbed onto the electrode-electrolyte interface. Specific adsorption is a phenomenon whereby ions are adsorbed to an amount greater than the charge on the electrode. Ions with higher association to solvent molecules tend to be less specifically adsorbed than the solvated counterparts. The outer Helmholtz layer forms at the boundary between the Gouy and the

inner Helmholtz plane. The solvated ions that cannot be specifically adsorbed, stay in the diffusion layer as illustrated in Figure 2.6.

#### *2.3.2.2.Equivalent circuit models of a supercapacitor*

Perhaps the most basic of SC models constitute 3 lumped elements: an equivalent series resistance, $R_{esr}$ connected in series to a conventional capacitor, C in parallel with another resistor, $R_p$ as depicted in Figure 2.7a [51, 52]. All the required parameters can easily be obtained from information presented in the data sheet of the manufacturers, making it very easy to simulate. The simplicity of this model is quite attractive however, it is unfortunately stymied by inaccuracies causing a mismatching SC behavior [51, 53]. A modification of this model uses an equivalent series inductor to account for the inductive lead in the SC as shown in Figure 2.7b [52]. To emulate SC performance in slow discharge applications, Cultura and Salameh proposed another model with easy parameterization [54], (Figure 2.7c).

In order to increase the accuracy of the simple classical models, the lather model, Figure 7d [51], transmission line model, Figure 2.7e [54], Zubieta model, Figure 2.7f [55, 56], and the Two branch model, Figure 2.7g [57, 58], were brought to light. However, all of them suffer from difficulties in parameter identification, since experimental data is required for their calculation. The Lather circuit model is based on a distributed parameter system, realized through a multitude of lumped parameters in a lather circuit. Other than the leakage resistance, parameters are determined via ac impedance measurements [51]. Similarly, since capacitance of an SC varies nonlinearly with available surface area, it can be modeled as a transmission line, with distributed voltage dependent capacitances as epitomized in Figure 2.7e. This model suffers from a myriad of undeterminable parameters, the exact number of which is yet to be identified for accurate modeling. Cultura and Salameh [54] proposed a simplified version, depicted in Figure 2.7c, modeling the SC terminal voltage. Zubieta's model [56] assumes that charging of a capacitor occurs in three phases each represented by an RC time constant. Parameter calculation also assumes that only certain sections of the circuit model are affected in different time instances. For example, charge is only stored in the immediate branch after 20 ms of charging.

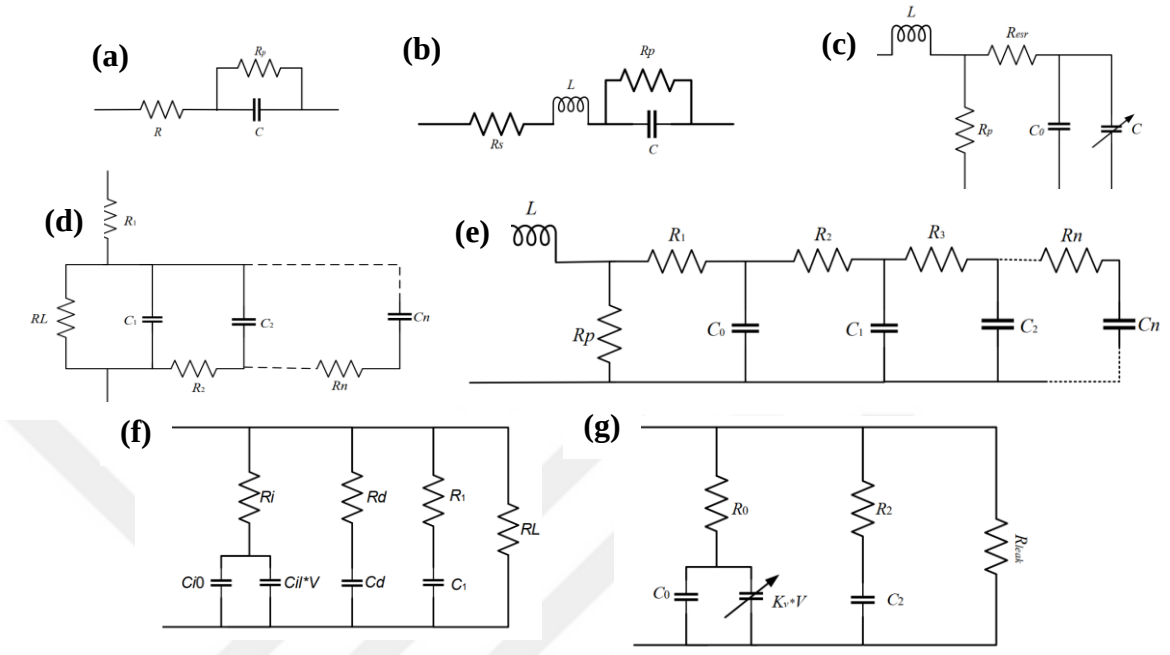


**Figure 2.7.** *Equivalent circuit models of a supercapacitor: (a) simplest model of an SC, (b) simplest model with inductive effect considered, (c) Cultura and Salameh model, (d) the lather model, (e) the transmission line model, (f) Zubieta model and (g) the two-branch model (Zhang L., 2018)*

Equivalent circuit models remain barely accurate, while maintaining their simplicity. More accurate models demand increase in parameters making it more convoluted to be calculated. Intelligent models are thought to be able to provide better performance. However, despite their precision, they are capacitor specific, and parameter identification is difficult and onerous [48, 59]. Other models such as the fractional order model, models for self-discharge and thermal behavior of SC, are discussed in a review by Zhang, L., et al [48].

### 2.3.3. Performance evaluation criteria for supercapacitors

Among many parameters two are ubiquitously considered when evaluating the performance of a supercapacitor. They are the energy storage capacity of the device and its power capability.

#### *2.3.3.1. Specific power and energy density*

The total amount of energy that a capacitor can store per unit mass of active material, at a given time is referred to as its specific energy. It is measured gravimetrically in units of watt-hour per gram/kilogram (Wh $g^{-1}$ or Wh $kg^{-1}$). Energy density on the other hand is the total amount of energy that can be stored in one-unit volume (usually calculated by

considering the total surface area of the electrodes multiplied by the thickness of the current collectors, separator and electrode materials [60]) of a supercapacitor. Its units of measurement are Watt-hour per centimeter squared (Wh $cm^{-2}$). For a double layer capacitor, the energy, E is calculated as in E.2.7 [34], where q is the total charge stored by the supercapacitor, $C_{dl}^{T}$ the double layer capacitance, and $V_{sc}$ the source voltage.

$$E = \int_0^q V_{sc}\,dq = \int_0^q \frac{q}{C_{dl}^{T}}\,dq = \frac{q^2}{2C_{dl}^{T}} = \frac{(C_{dl}^{T}V_{sc})^2}{2C_{dl}^{T}} = \frac{1}{2}C_{dl}^{T}V_{sc}^2 \qquad (2.7)$$

The more practically useful specific energy is given by E.2.8, with $E_m$ being the specific energy of the capacitor measured with respect to the mass of the active material m.

$$E_m = \frac{1}{2}\frac{C_m}{m}V_{sc}^2 = \frac{1}{2}C_{sp}V_{sc}^2 \qquad (2.8)$$

#### *2.3.3.2.Specific power and power density*

Specific power refers to the rate at which energy per unit mass/volume, is delivered from or absorbed by a capacitor. The best analogy is that of a water tank, with a hole at the bottom. The bigger the hole, the faster the water flows out and the faster the tank empties. Capacitors generally can only store a small amount of energy but regardless, they deliver this energy at very high speeds. Specific power is measured in kilowatts per kilogram (kW $kg^{-1}$) or in kilowatts per cubic centimeter (kW $cm^{-3}$). The specific power of a capacitor is calculated as in E.2.9 [61]. V is the capacitor's voltage window, $R_{es}$ the equivalent series resistance, m the mass of the active material and $v$, the volume of the capacitor.

$$P = \frac{V^2}{4mR_{es}} = \frac{V^2}{4vR_{es}} \qquad (2.9)$$

### 2.3.4. Differences between a battery, supercapacitor and a fuel cell

The difference between an SC and other energy storage technologies are best outlined in a study by Conway [1, 13], however the most salient differences, being in energy storage mechanism, energy and power capabilities, charge rate and life, can be represented in a Ragone plot (Figure 2.8) [33].

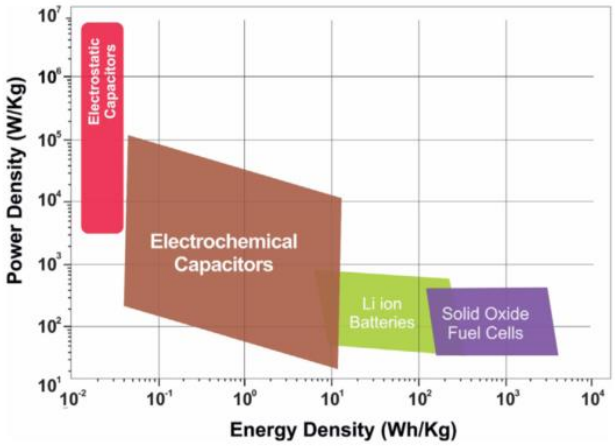


**Figure 2.8.** *Ragone Plot energy storage systems: Capacitors, SCs, Li-ion Batteries and Fuel Cells (Raza, 2018)*

Energy storage in batteries happens via chemical redox changes in the battery whereas SCs store energy by electrostatic charge accumulation and or fast redox reaction and doping [13]. Although batteries can store more energy than SCs, the rate at which this energy can be delivered is seriously limited. The charge rate of batteries is limited by the speed of redox reactions, whereas for SCs it is dependent on electrostatic charge gathering and is comparable to the normally high discharge rate. While batteries only have a life cycle of about 500 hrs., SCs can live for 30,000 hours to 1 million hours. and can be charge in durations of 1–10 s vs. 10–60 min compared to the former [62]. The thermal stability of SCs is be tunable and ranges between − 40 and 100 °C, on the contrary batteries one operate within a temperature range of − 20 and 60 °C [33, 63].

### 2.3.5. Applications of supercapacitors

The high-power density of supercapacitors and their ability to withstand many charge-discharge cycles, render them auspicious for applications in a variety of fields ranging from consumer electronics, power grid, medical, transport to military. SCs are best employed in applications with energy requirements in the time range of 1 ms and 100 s [23].

Most contemporary commercial SCs have seen usage in consumer devices, backing up microcomputers, system boards, clocks and memory devices [23]. SCs can be employed in devices where load fluctuation is a thorn in the eye. Renewable energy systems such as wind and solar, exhibit fluctuating sources caused by gusting or clouds. SCs can easily remedy this

by stabilizing grid voltage and frequency, balancing power demand and supply and managing real or reactive power [64, 65].

The emergence of electric-powered devices has opened doors for the application of SCs in fields with high energy throughput requirements such as hybrid electric vehicles and those requiring stable energy throughput as is the case with sensitive automation, computer chips and portable electronics. This is due to the long cycle life and short charging time enjoyed by SCs [66].

### 2.3.6. Research approach in SC technology

Though enjoying high power densities, SCs usually pale in comparison to Li-ion batteries when it comes to energy density. This has stemmed ubiquitous applications of the SC as an alternative to the battery. To curb this shortcoming, research in SC technology has progressed in different directions. Material, architecture and electrolyte design have received the most research attention, focusing on improving supercapacitor performance.

#### *2.3.6.1. Active material design*

The capacitance of a capacitor is directly proportional to the surface area of the electrode material (see E.2.1). Inspired by this fact, a bulk of research resources are devoted to designing electrode material with appropriate structures conducive for better electron transport and ionic diffusion [67]. The path of this technology can be traced from 3D or bulk carbon or carbon-based materials to 0D quantum materials [68, 69]. Research on carbon and carbon derivative materials for EDLC application mainly focuses on tuning the pore sizes as the ratio of the pore size to electrolyte ion size is pertinent in determining the device's capacitance capability [70, 71].

To compound capacitor performance, ample research funds have been allocated to developing nano porous materials with increased effective surface area [72, 73]. An example by You, B., et al. [74], demonstrates a homogeneous deposition of $MnO_2$ nanorods on GO (graphene oxide) to mitigate restacking of RGO layers incurred during processing. This resulted in a boast in effective surface area as well as a shorter ionic diffusion path. Improving the wettability of the electrode surface in contact with the electrolyte is another approach to increase SC performance. GO for example houses redox active oxygen-based functional groups capable of increasing the total active area of the SC by providing pseudo capacitance

as well as improving the wetting of the active material with the electrolyte [75]. Another enhancing approach to SC performance is adjusting the mass transport mechanism, as higher mass transport tantamount to increased capacitance. H. Wang et al., demonstrated this by fabricating a graphene–nickel cobaltite nanocomposite/activated carbon (AC) hybrid material with a mass loading of 10 mg $cm^{-2}$ achieving a capacitance of 618 F $g^{-1}$ [33, 76].

Searching for better electrode materials is one of the easiest ways to foster SC capacitance. In this light, the advent of 2D materials has spurred colossal research attention to their potential for application in SC electrodes due to their peculiar electrochemical properties [69]. Graphene, Phosphorenes, MXenes, TMDCs and TMO/TMHs are the contenders in the 2D family for application in SC electrodes. Albeit high performance at single or fewer layers in thickness, 2D materials tend to exhibit inferior capacitances due to agglomeration. One remedy is ion intercalation which not only can alleviate restacking but increase the electrode's conductivity as well, improving the power density which is contingent upon the material's resistivity [77].

This section only highlights general research proceedings in material design, however more detailed information can be found in review studies [33, 67-69].

***2.3.6.2.Design of the electrode***

The oldest and most basic SC designed described by Conway [1], constitutes two electrodes (a metal current collector, one side of which is covered by an active material) aligned with an electrolyte-soaked separator in between. Tuning of the electrode separation in this structure is limited as the leakage current also increases with decrease in separation distance. Ion diffusion path is also longer and in a dilapidated state for pseudo active materials.

Micro supercapacitors (MSCs) in planner architecture [78] are also a focus of studies as they possess the benefits of decreased ion diffusion paths, no separator requirement and ease of integration in microchips. Research in MSCs mostly focuses on the design methodology rather than the design itself. Direct laser writing [79], photolithography [80] and printing are some of the methods used. 3D on chip MSCs are also gradually drawing research attention [81, 82]. The 3D matrix of electrodes is supposedly capable of boasting

energy density as well as reducing inter electrode ion transport. Fiber type MSCs are also captivating designs in SC research for miniaturized portable and wearable electronics [83].

Another design aspect that has charmed its way into the SC world is flexibility, which is desired for integration in flexible and wearable electronic devices with aesthetic appeal and multifunctionality [84]. Flow SCs, ac line-filtering SCs, redox electrolyte enhanced SCs and metal ion hybrid SCs are some of the design structures under investigation [67].

#### *2.3.6.3.Electrolyte*

It is obvious from E.2.8 that increasing the voltage window of an SC will dramatically raise both its power and energy density. What determines this voltage window is the electrolyte which is only stable within a certain voltage range [85]. One of the drawbacks of SC technology, the scarcity of highly conductive materials can be remedied by designing ionic electrolytes [68]. Electrolyte design has mainly focus on the design of aqueous, organic, ionic liquids, solid-state or quasi-solid-state and redox-active electrolytes. A more elaborate study on electrolytes is give on reviews by Raza, W., et al., and Zhong, C., et al., [33, 85].

#### *2.3.6.4.Reducing the manufacturing cost*

The final goal of every research is commercialization; however, one of the factors rendering SCs less competitive to batteries is their cost of manufacturing. As the performance of electrode materials is seamlessly optimized via research, the ubiquitous deployment and commercialization of SCs calls for increased research to lowering their manufacturing cost [86]. A study by Andrew Burke's revealed that, carbon is responsible for about 60% of the total materials cost, resulting in a total electrode material cost of 0.1 ¢ $F^{-1}$. Biochar-derived electrode material on the other hand costs only 0.001 ¢ $F^{-1}$ [33, 87]. Biomass and natural polymers are topping the list of precursors for carbon-based SCs as a result of their economical and sustainable advantages [88]. One main drawback is the activation method which usually employ high cost chemicals which also adversely affect the materials final properties. Researching on alternative low cost activation methods could greatly lower the device's final cost [33].

The manufacturing process of carbon-based materials is usually a convoluted one involving the use of binders which cause agglomeration and increased resistivity, inducing the need for conductive promoters. All this only serve to increase the total cost of final

product. This has coerced enormous research into the production of binder free carbon electrodes with the hope of lowering manufacturing cost [89].

### 2.3.7. Challenges faced by SC technology

The main challenge faced by SCs is that of poor energy storage capability making them less competitive with Li-ion batteries. Upon trying to optimize one parameter, the effectiveness of the other becomes diminished. Materials used for EDLC tend to possess high power densities as well as long life whereas pseudo active materials can store more energy. There is always a tradeoff to be made for example trying to increase the energy storage capability of EDLC via hybridization leads to a lost in power capability and durability.

Little research attention has been given to developing novel electrolytes and as a result, the current electrolyte technology has not caught up with contemporary material design. With the advent 2D nanomaterials possessing surface atoms endowed with novel physiochemical, the demand for new compatible electrolytes has become unavoidable. MXenes for example easily oxidize in various aqueous electrolytes, causing increased resistance and reduce cycle life [90]. Phosphorenes are prevaricated by stability crisis under normal ambient conditions and for this reason assembling of phosphorene supercapacitors has to be done in an inert environment [91]. One proposed solution is proper encasement or functionalization of phosphorenes while maintaining their electrochemical properties [69].

## 2.4. Original Contributions and Motivation

Discovering an ideal material with intrinsic excellent electrochemical properties is the dream of every energy researcher. However, such a material is yet to be discovered and there is always a tradeoff to be made- so far materials used in electrode design usually possess only one aspect of the desired property. For example, carbon -and carbon- based materials are endowed with high power density capabilities but cannot store much energy. Pseudo active materials however have the capacity to store more energy but are rather slow and are met with high resistances, thus lower power densities. To mitigate this conundrum, research has strived to hybridize these materials in an attempt to synergize their benefits and curb their shortcomings [32].

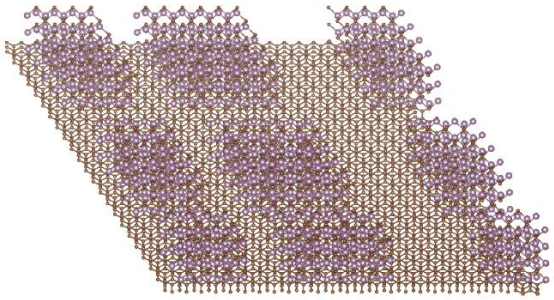

**Figure 2.9.** *The structure of a MXene-Graphene composite*

Graphene has a high surface area and is also highly conductive [66, 92, 93], while MXenes are electrophilic providing for better wettability, and have large interlayer spacings allowing for ion intercalation [94-96]. By hybridizing these two materials as illustrated in Figure 2.9, we endeavor to improve their performance by combining their individual beneficial properties. Layer agglomeration is also expected to decrease with this hybrid configuration.

# 3. CHEMICAL VAPOR DEPOSITION OF 2D MATERIALS

Chemical vapor deposition (CVD) a process whereby a solid material is deposited from vapor phase precursors via a chemical reaction on or in the vicinity of an appropriately heated substrate surface. The output of this process usually takes the form of a thin film, powder, or single crystal. By playing with experimental parameters such as substrate material type, substrate temperature, precursor concentration, carrier gas rate, total pressure gas flows, etc., materials with a wide range of physical, tribological, and chemical properties can be grown. The most salient feature of CVD is its excellent throwing power, conducive to uniformly thick coatings and properties with a low porosity even on convoluted shaped substrates. CVD is also capable of localized, or preferential deposition, on patterned substrates [97].

## 3.1. Graphene

Myriad methods are used to prepare graphene ranging from mechanical exfoliation (produces graphene with the highest quality, however has neither high throughput nor high yield [98]), PECVD, CVD [99], chemical methods (e.g. liquid phase exfoliation), thermal decomposition of SiC, unzipping of CNT etc. [100]. Compared to other methods, CVD has a flush of merits such as repeatability and control of grain size and layer number as well as mass production as demonstrated by Bae, S., et al. [101].

### 3.1.1. Chemical vapor deposition of graphene nano-sheets.

The graphene used in fabricating our supercapacitors is grown in our home-built CVD system, the schematic of which is shown in Figure 3.1. As illustrated in the figure its components are an 80 cm diameter tube sealed at both ends by removable flanges, a vacuum pump for pressure control (not shown in the figure) and a gas supply unit fed through mass flow controllers (MFCs) calibrated for specific gases. Also included in Figure 3.1 is the standard setup for our graphene growth experiments. Our substrate of volition is copper for its catalytic effect, conduciveness for high coverage deposition (95%) [102] and its conformity with our preferred transfer method.

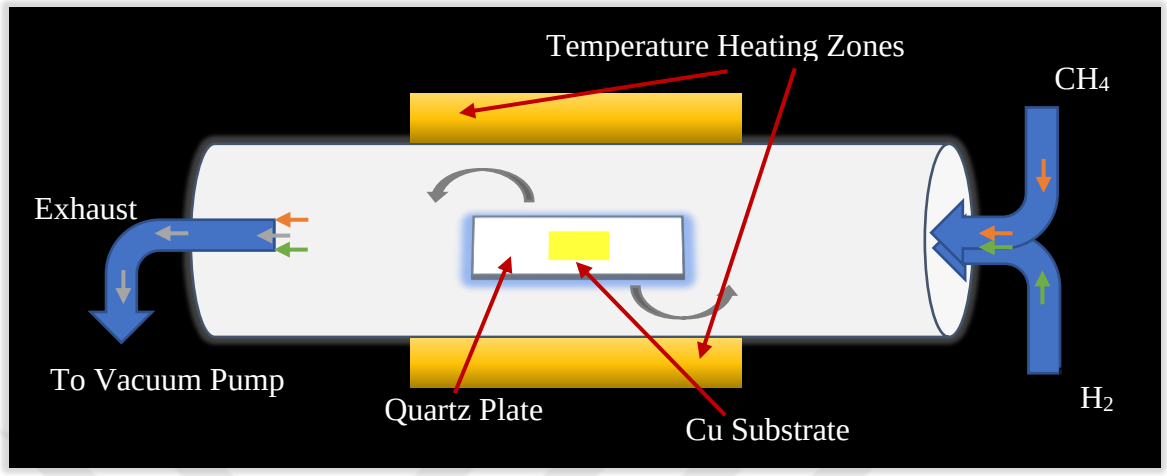


**Figure 3.1.** *CVD setup for growth of graphene*

Growth experiments are observed under vacuum (~1.0 torr) at a temperature of 1035 $^{0}$C ramped at the highest rate of the reactor. The gases are supplied at a rate of 100 and 40 standard cubic centimeters per minute (sccm) of $H_{2(g)}$ and $CH_{4(g)}$ respectively, with $CH_{4(g)}$ introduced only at 1035 $^{\circ}$C for the duration of the experiment. Growth time varies depending on the intended number of layers of graphene, from 2 mins, 45 sec to 5 mins. To obtain a continues film of monolayer graphene we used 2 mins 50 sec below which we obtained a fully covered substrate with monolayer graphene.

### 3.1.2. Material characterization methods.

The as grown samples are characterized by optical microscopy, Raman spectroscopy, atomic force microscopy and resistivity measurements. Optical characterizations are done using **Nikon Eclipse LV100NDA** optical microscope, whereas Raman spectra are obtained using **WITec alpha-300R,** and while AFM measurements are taken with a portable **NanoMagnetics-ezAFM™** suit.

#### *3.1.2.1. μ-Raman and Photoluminescence*

Raman spectroscopy is a technique used to identify frequency unique properties (fingerprint) of a material. It involves the irradiation of a test sample by intense laser beams in the UV-visible region. Upon interaction with the sample, the irradiated light gets scattered in a direction usually normal to the incident beam. One of the scattered light experiences elastic scattering (also called the Rayleigh scattering ($v_0$)), which is strong and has the same frequency as the incident beam. The other undergoes inelastic scattering (Raman scattering)

is very weak (~ $10^{-5}$ of the incident beam) and has frequencies $v_0 \pm v_m$, $v_m$ being the vibrational frequency of a molecule. Vibrations with frequencies less than Rayleigh, $v_0 - v_m$ are called the Stokes while the others with higher frequencies, $v_0 + v_m$ are known as anti-Stokes lines. Therefore, in Raman spectroscopy, the vibrational frequency ($v_m$) is measured as a shift from the incident beam frequency ($v_o$) [103].

The Raman spectra of specimen is obtained by collecting and dispersing the scattered light onto a charge coupled device, the CCD detector. The dispersion of the scattered light is done by optical diffraction gratings which splits the incident light into several beams. The gratings differ in resolution for e.g. **WITEC alpha300R** Raman has 300, 600 and 1200 grooves per millimeter (g $mm^{-1}$). The Raman and PL spectra in this work are mostly obtained using the 300 g $mm^{-1}$ and 1200 g $mm^{-1}$. The incident light is filtered by an edge filter before interring the grating. The laser beam is focused onto the slide by optical microscope with different magnifications and numerical aperture values (NA), whose spatial resolution is proportional to the ratio of wavelength of the excitation and the NA ($\lambda$/NA). For example, the spatial resolution of the 100x objective is between 400 nm to 500 nm and depth resolution ($\lambda/NA^2$), in the order of 1 μm. The optical microscope used for the Raman Spectroscopy of this dissertation is configured as 50x and 100x objectives with 0.87, 0.9 NA respectively, and a continuous wave (CW) laser of wavelength 532 nm coupled to and a CCD detector.

The properties of layered materials such as the number of layers, coulombic interaction, electron doping level, adsorbates and crystal quality, are catholically determined by analyzing their Raman and/or PL spectra. For example the number of layers in a graphene (i.e. monolayer, bilayer up to around 4 layers) can be correctly surmised by examining the ration of 2D or G' and G Raman mode peak intensities (for example $2D/G \geq 2$ for monolayer graphene) and the FWHM of the Lorentz fitted 2D vibrational mode [104]. The thickness estimation of TMDCs on the other hand, is done by evaluation of peak positions of the fundamental Raman modes. For example, the frequency difference between the in plane ($E^1_{2g}$) and out-of-plane ($A_{1g}$) in the case of $MoS_2$ and the location of their peaks for $MoSe_2$. For $MoS_2$, the $E^1_{2g}$ results mainly from the out of plane vibration of S atoms, whereas $A_{1g}$ is used to evaluate monolayer materials properties. The $E^1_{2g}$ mode usually shifts towards higher frequencies, with the $A_{1g}$ mode moving towards lower wavenumbers as the number of layers

increase [105-107]. A more detailed background of Raman and PL spectroscopy of 2D materials can be found in previously reported literature [103, 108, 109].

### 3.1.3. Observation and discussion

Our grown samples are transferred onto Si substrates that is coated with $SiO_2$ (300 nm). Optical images as well as dark field images of the sample are taken before and after transfer as shown in Figure 3.2a-b. To roughly estimate the number of layers of the as-grown graphene, we took single Raman spectra, depicted in Figure 3.2c. The ratio of the G' or the 2D peak to the G peak intensity is 1.997 and after fitting the spectra with the Lorentzian function, we measured the FWHM (full width half maximum) of 25.1 $cm^{-1}$ which is in close conformity with previous reports (~24 $cm^{-1}$), indicating monolayer graphene [110]. The presence of some multilayer islands was observed thus, to measure their concentration, we took line and image scans across the sample. AFM recorded a step height of ~0.3 nm conforming with literature reported values [111].

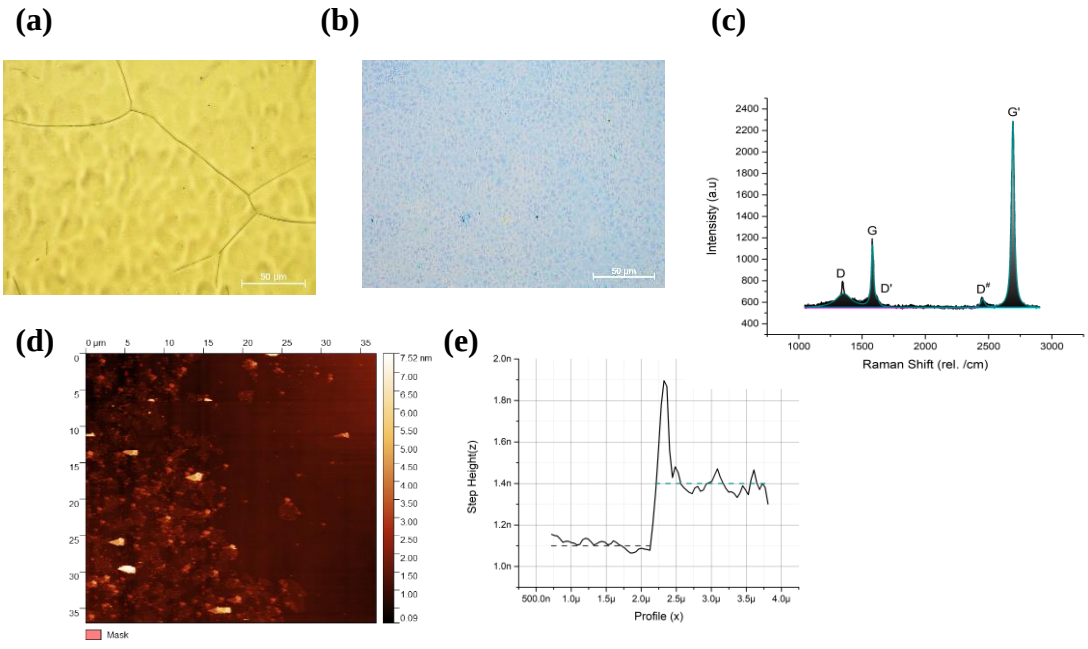


**Figure 3.2.** *Optical characterization of CVD grown graphene: (a) Image of as grown graphene of Cu substrate, (b) Graphene transferred onto Si/$SiO_2$ substrate, (c) Raman spectra of graphene, (d) AFM image showing the topography of graphene on Si/$SiO_2$ and (e) Step height of graphene measured from the AFM results.*

## 3.2. Transition Metal Dichalcogenides, TMDCs, On Glass Substrates

CVD growth of TMDCs, especially $MoS_2$, prevails modern research in 2D materials due the ease in which they can be grown. Research in the growth of TMDCs has almost reached maturity and is getting ready for commercialization. By changing growth configurations, various sizes of TMDC domains can be grown in a controlled and repetitive manner. Also, the alignment of the triangular TMDC crystals, such epitaxial arrangement, can be achieved. Apart from this, the coverage area of the flakes can also be controlled such that uniform and large area films can be grown. Successful synthesis of different TMDC phases such as 1T metallic and the 2H semiconductor phases has also been realized. In our lab, we can grow $MoS_2$, $MoSe_2$, $WS_2$ and $WSe_2$ on both Si and on soda lime glass substrates. This section focusses only on TMDC synthesis on glass substrates.

### 3.2.1. Chemical vapor deposition of $MoS_2$

High affinity between Mo and S atoms makes $MoS_2$ one of the easier TMDC materials to grow, without the need for a reducing agent such as $H_2$. CVD is widely investigated due to its conformal film, high purity deposition of a variety of materials, high deposition rates and no high vacuum requirements [112]. In another direction, various materials such as $SiO_2$/Si, quartz glass, sapphire [113], polyimide(PI) [114] etc. are used as substrates for the growth of these 2D materials.

The synthesis of graphene on molten metallic substrate allows for hexagonal crystallites to assembled in a highly aligned manner [115], thus inspiring exploration of other molten substrates. Crystallite nucleation tends to occur preferentially at impurity sites of solid substrates, imploring the use of complicated substrate treatments or growth techniques for quality synthesis [116]. Molten glass offers a low-defective and isotropic surface with a low nucleation density allowing for deposition of large crystalline domains [117]. Apart from the afore mentioned, soda lime glass contains $Na^+$ ions, known to catalyze the growth of large sized and oriented monolayer TMDCs flakes [113, 118]. In the synthesis of $MoS_2$, as temperatures increase, $Na^+$ ions react with Sulphur to form $Na_2S_x$ ($x>1$) which has strong affinity for $O_2$ and $H_2O$, thus the Na-promoted oxidation. $Na^+$ reacts with Mo and S to form an intermediate solution of $Na_2S_x.MoS_2$, Na located at the Van der Waal spaces. This

intermediate solution is unstable and decomposes into $MoS_2$ upon exposure to air, as Na reacts with air to form $Na_2CO_3$ and $NaCHS.2H_2O$ [119, 120].

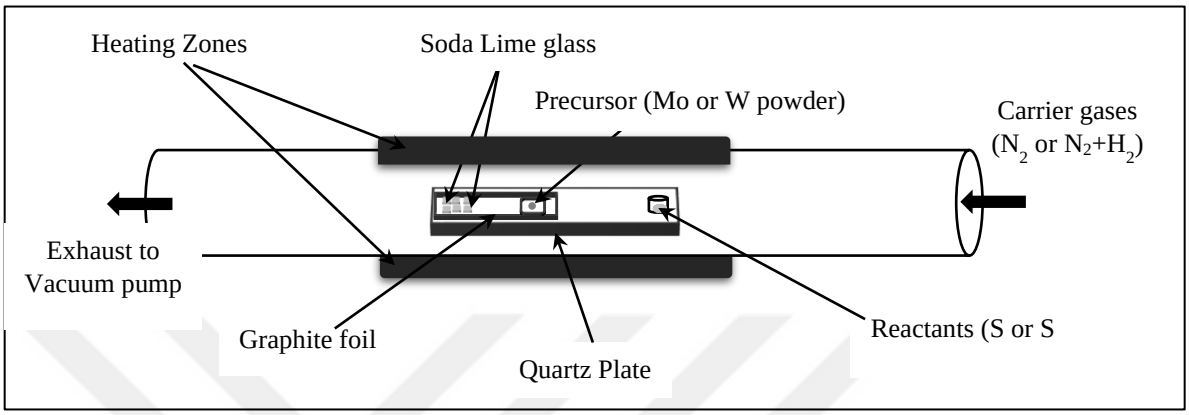


**Figure 3.3.** *CVD setup for growth of TMDCs*

All our TMDCs are grown using the same general CVD configuration, illustrated in Figure 3.3, with slight material specific differences. We use 80 mm and 70 mm diameter tube reactors, supplied with $N_2$ or $N_2$+$H_2$ depending on the material. Six (20x20x0.16 mm) or two (76x26 mm) glass substrates are placed on a graphite foil – to prevent glass cracking-. The metallic precursor is place 4 cm from the front edge of the substrate, whereas the chalcogen is placed 15 cm from the metallic precursor.

Using a face-up approach (crystal grown this way are more stable [121]), different growth recipes are optimized depending on desired material, from a continuous monolayer film to evenly distributed flakes. Soda lime glass substrates are first cleaned by 5 mins ultrasonication with acetone, Isopropanol and Deionized water, in that order, followed $N_2$ drying and 2 minutes baking on a hot plate at 105 °C. $MoS_2$ of approximately same size evenly distributed throughout the substrate are grown using the 70 mm tubed reactor. 300 mg of 99.98% S (Sigma Aldrich) and ~0.5 mg of $MoO_3$ powder (99.95% Sigma Aldrich) placed as shown in Figure 3.3, are used to synthesize $MoS_2$ under atmospheric pressure (i.e. ~750 torr) at a temperature of 750 °C. 150 sccm of $N_2$ carrier gas is used for the growth of $MoS_2$ using the 70 mm tubed reactor whereas 300 sccm is used for the 80 mm tube, every other parameter kept the same. By varying the concentration of the metallic precursors, we can control the size as well as the coverage of grown material.

### *3.2.1.1.Characterization of $MoS_2$*

Samples grown by CDV technique are characterized by Optical microscopy, Raman Spectroscopy, Photoluminescence and Atomic Force Microscopy.

### *3.2.1.2.Results and conclusions*

Optical imagery on as grown samples illustrates different growth mechanism depending on the diameter of the tube used (Figure 3.4). Samples grown in different reactors under same conditions, with the only difference being the $N_2$ flow rate (i.e. 150 sccm for the 70 mm and 300 sccm for the 80 mm diameter tubed reactors respectively, optimum for $MoS_2$). With high concentrations of $MoO_3$ metallic precursor (>0.5 mg) synthesis of continuous monolayer film of $MoS_2$ is realized (Figure 3.4a) and at slightly lower concentration (~0.5 mg) crystal sizes of ~800 µm were grown (Figure 3.4b). Control of crystal size is further illustrated by Figure 3.4 c, d and f, with sizes of ~400 µm, ~150 µm and ~40 µm respectively. Nucleation sites that are closer to each other lead to crystal amalgamation at the edges as shown in Figure 3.4d. However, the dark field image (Figure 3.4e) suggests no overlapping of crystals, further confirmed by Raman spectroscopy, showing the same peak position difference of 19 $cm^{-1}$.

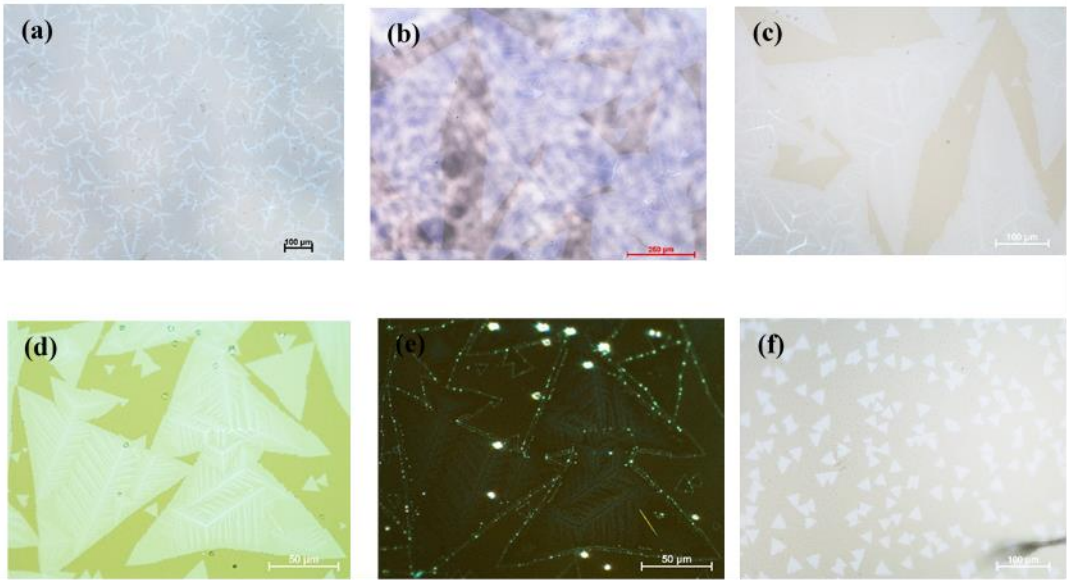


**Figure 3.4.** *Optical images of $MoS_2$ grown on glass substrates: (a) continuous film, (b) $MoS_2$ crystals with domain sizes averaging 800 µm, (c) 400 µm edged crystals, (d) 150 µm $MoS_2$ flakes, (e) Dark field image illustrating amalgamation and second layer nucleation, (f) Tinny crystals, ~40 µm, at low concentrations of metallic precursor and furthest from the precursors*

Different concentrations of $MoO_3$ (0.1 to 1 mg) metallic precursor (every other parameter being constant) results in growth of $MoS_2$ crystals films, triangular flakes, and isolated crystals. Optical images taken at different distances from the edge of the substrate closest to the precursors give information about the domain size variation in different sized tubes as seen in Figure 3.4. It was also observed that two (26x76 mm) or six (or 6 20x20 mm) substrates juxtaposed, experience growth differently. Considering the flow direction of the carrier gas, the substrate on the right-side favor perfectly rectangular crystals, whereas the left entertains crystals with a more distorted triangular shape similar to a 3-pointed star. In an experiment using ~0.1 mg of $MoO_3$ precursor, a film of $MoS_2$ (with multilayer regions) was observed at 0.2 cm into the substrate, in the direction of gas flow. At 1 cm, the crystals begin to separate; however, still merged at the edges. At 2 cm, though still merged, crystal edges can be traced and the distance between them also increases. As the we move deeper into the substrate at 3 cm only the tips of the crystals touch each other and crystal domains average ~142 μm. 4 cm more, the crystal sized decreases to ~115 μm and the pine-shaped (indicative of the nucleation of the second layer) apparitions on the surface of the crystals begin to make way for more perfect monolayer crystals. 70 μm crystal domains free of pine-like growths are observed at 5 cm and 60 μm at 6cm with some amalgamated in a butterfly structure. At 7 cm the average crystal size shrinks however crystals measuring 143 μm could still be spotted. Crystals on the left substrate more evenly distributed with grains averaging 103 μm at 0.1 cm and 82 μm at 7 cm with the only difference being in the separation between crystal grains and their clarity. Crystal domains furthest away from the precursor are free from second layer nucleation and are sparsely distributed with tiny crystal dotted in-between. The absence of a film area on the left substrate suggest that the right side favors the growth of a monolayer $MoS_2$ with layer and size control.

While crystals grown using the 70 mm diameter tubed reactor permits slight variations, grains sizes vary markedly along the substrates as well as substrate's placement (left or right). An experiment conducted with 0.1 mg of $MoO_3$ precursor; 300 sccm of $N_2$ and at 800 °C, showed growth of a film of $MoS_2$ at the edge of the substrate closest to the precursor. 1 cm into the substrate saw disintegration of the film, flakes at further distances, sizes ranging from 315 μm via 175 μm midway to negligible sized crystals from 6 cm in the substrate and onwards. The left side witnesses a rather uniform distribution of crystals up to the middle of

the sample (59 μm through 31 μm to 1.6 μm at 4.5 cm). Observations from several experiments suggest that carrier gases tend to flow more to the right, explaining why it experiences a relatively high deposition.

Optical characterization results are shown in Figure 3.5. The difference between the in-plane and the out-of-plane Raman modes, ( Raman spectra in Figure 3.5a), was measured as 18.7 $cm^{-1}$ (Figure 3.5a), and this agrees with previous studies [122, 123]. Lorentzian fitting reveals the full width half maxima (FWHM) of 4.28 and 5.12 for the in-plane ($E^1_{2g}$) and out-of-plane ($A_{1g}$) Raman modes respectively. Figure 3.5b shows the image scan of the transferred samples after filtering the area with $A_{1g} - E^1_{2g} < 20$, suggesting high quality crystals of the as-grown $MoS_2$. The PL spectra measured from the transferred sample (Figure 3.5c) shows the Trion ($A^-$) at 1.8 eV, A exciton at ~1.84 eV and the B exciton at 1.96, further confirming mono layer $MoS_2$ [124-126]. The AFM results depicted in Figure 3.5d-e, show average roughness of 4.15 nm and a step height measured to be ~0.72 nm (Figure 3.5e), which closely conforms with previous studies [127].

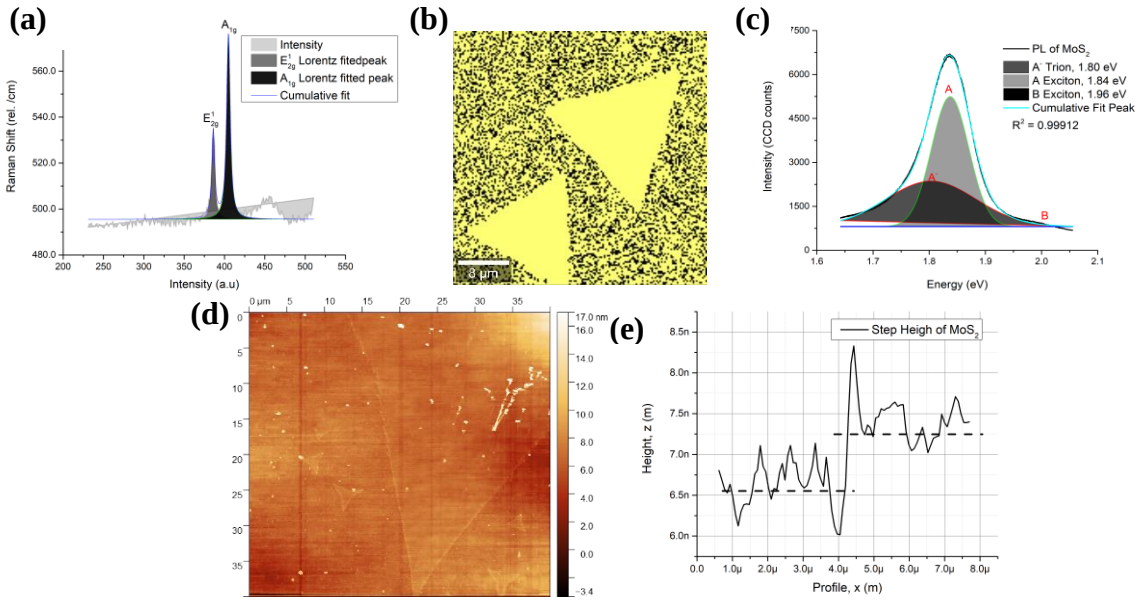


**Figure 3.5.** *Optical characterization of $MoS_2$: (a) Raman spectra results, (a) Filtered Raman image scan showing uniform monolayer crystals, (c) Photo luminescent of $MoS_2$, (d) AFM image showing the topology of the monolayer crystal, (e) Step height estimation from the AFM scan results.*

### 3.2.2. Synthesis of $MoSe_2$

Like $MoS_2$, $MoSe_2$ is a member of the 2D TMDC family with trilayers of molybdenum atoms sandwiched by two selenium atoms in a trigonal prismatic bonding. $MoSe_2$ vies for better properties with $MoS_2$ and has prevailed in terms of electrical conductivity due to the intrinsic metallic nature of Se ($1x10^{-3}$ $sm^{-1}$ compared to $5x10^{-28}$ for S) [128, 129]. Its layered structure and size are conducive for storing ions in energy storage applications like supercapacitors, Li and Na-ion batteries.

#### *3.2.2.1. Observation*

Chemical vapor deposition of $MoSe_2$ is somewhat like that of $MoS_2$ however, due to inferior reactivity of Mo with Se, $H_2$ is implored as the reducing agent. Figure 3.6 illustrates the optical images of $MoSe_2$ grown with different ratios of $N_2/H_2$. Most of our experiments were conducted using 0.5 mg of $MoO_3$ and 300 mg of Se and 20 sccm of $H_2$ at a pressure of 750 torr and 750 – 900 °C. Using various amounts of $N_2$ while keeping every other parameter the same resulted in different crystal morphologies of '$MoSe_2$', intimating of two or more crystals merging. At $N_2$ rates greater than 20 sccm, we obtained star-shaped crystals, as depicted by Figure 3.6a-b, on glass and transferred onto $Si/SiO_2$ substrates respectively. At 20/20 $N_2/H_2$ we obtained perfectly triangular crystal grains with ~30 μm average domain length as shown in Figure 3.6c. This experiment was not repeatable as we discovered that an explosive reaction would occur when the reactor temperature is between 550 – 560 and the precursors and substrates would be displaced. At this temperature range, $H_2$ whose concentration is high (20 sccm) reacts with $O_2$ (since our experiments were conducted at normal atmospheric pressure) to form $H_2O$ in an explosive reaction. To curb this, we adopted two strategies which resulted in different results. In one case $H_2$ was only introduced when the temperature of the experiment reached between 555 and 560. This resulted in triangular flakes similar to those shown in Figure 3.6c, and they were evenly spread over the substrate. Strangely no growth was observed if $H_2$ was applied at temperatures above 590 °C or at growth time as suggested in previous studies [117]. This is because an intermediate reaction between the reactants occur at this temperature range and require the reducing effect of $H_2$ [120]. The other approach was to introduce a small amount of $H_2$ (3-7 sccm) at the start of the experiment as $N_2$. Figure 3.6d-f illustrate crystals grown using 95 sccm of $N_2$ and 5 sccm

of $H_2$. This recipe was conducive to the growth of a continues film of $MoS_2$ (Figure 3.6d), flakes ranging from 715 µm (Figure 3.6e) via 414 µm (Figure 3.6f) to 10µm as we moved further away from the precursors on the substrates.

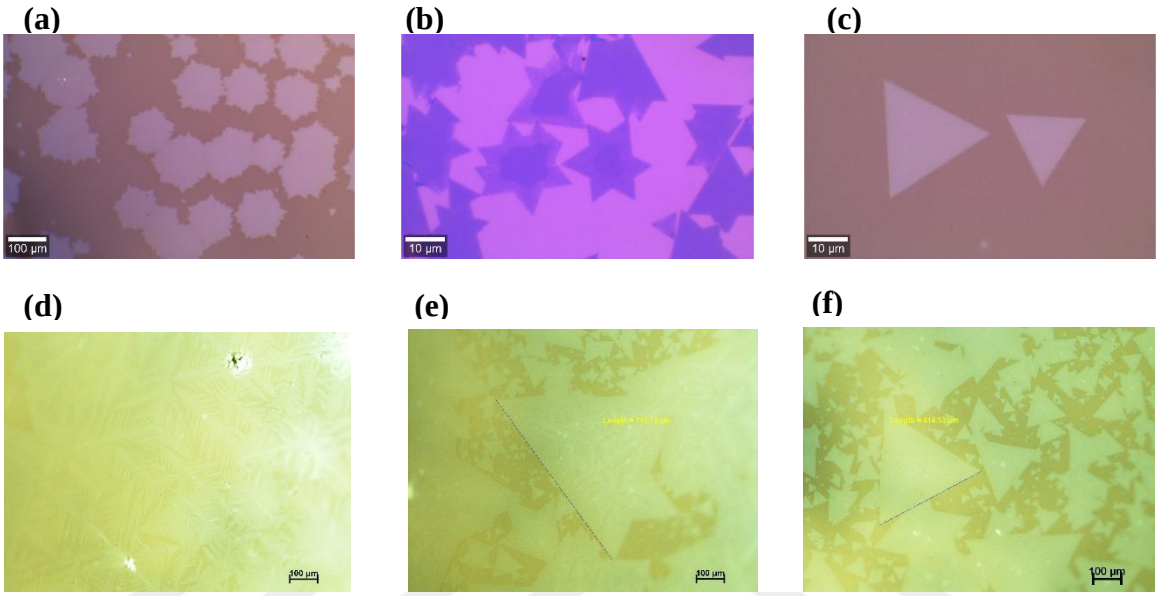


**Figure 3.6**. *Optical images of '$MoSe_2$' crystals: (a) Multi-edge shaped crystals on glass substrates, (b) Image of flakes transferred onto Si/$SiO_2$ substrate, (d) Continuous film of $MoSe_2$ crystal, (e) $MoSe_2$ crystal with an edge length of 715 µm, (f) Flake with domain size of 414 µm*

### *3.2.2.2.Characterization and discussion*

All CVD samples were characterized by Raman spectroscopy, Photo Luminescence (using 530 nm laser) and Atomic Force Microscopy. Figure 3.7a illustrates the Raman spectra of monolayer $MoSe_2$ in harmony with previews studies [117, 130]. A sharp peak allocated to the out-of-plane vibration mode ($A_{1g}$) is observed at 238.7 $cm^{-1}$ and the in-plane ($E^1_{2g}$) mode at 270 $cm^{-1}$.

The Raman spectra of as grown '$MoSe_2$' on glass substrates indicated two sharp Raman active modes one at 223 $cm^{-1}$ and another at 263 $cm^{-1}$ with a position difference of 40 $cm^{-1}$ (Figure 3.7b), incongruous with the previously obtained results [117, 130]. As shown in Figure 3.6b, the appearance of another vibration mode at 239.6 $cm^{-1}$ indicates that the $MoSe_2$ is a monolayer. Although the origin of the two peaks is still unknown, two propositions have been made. One claims the possibility of the crystal having undergone a phase transition to 1T $MoSe_2$ which can be able to explain the non-stability of these crystals (it was observed

that the flakes decompose with time upon exposure to the air). This theory was debunked by their poor performance in FET applications. The second hypothesis suggests an alloy, $MoS_xSe_{(2-x)}$ claiming the contamination of the CVD system by Sulfur ($MoS_2$ and $MoSe_2$ are synthesized in the same CVD system only changing the tubes). According to Jadczak, J., et al. [131], the $A_{1g}$ Raman mode of $MoSe_2$ begin to split as the Sulfur composition, $x \leq 2$ in the $MoSe_{(2-x)}S_x$ increases. They further elucidated that the origin of the peak splitting is due to the presence of S atoms that create a dipole moment in the system and in turn causes polarization of the $MoS_xSe_{(2-x)}$ molecule as opposed to coherent vibration of pristine $MoSe_2$ layers. This is the closest explanation to the Raman spectra of $MoSe_2$ on glass substrates of Figure 3.7b. The big question now is "where does the S come from?". Using the same CVD system under the same conditions, we performed NaCl assisted growth of $MoSe_2$ on $Si/SiO_2$ substrates and obtained crystals with Raman spectra as in Figure 3.7a. This proved that the contamination was not from the system. The only suspect now is the glass substrate itself. A study by Williams et al. [132] revealed the presence of about 0.01 to 1% of $SO_3$ on glass backing the claim that the peak splitting is originating from S contamination. However more research need to be done as there still exist subtle differences in the Raman peaks when compared with the $MoS_xSe_{(2-x)}$ Raman modes. Only by analyzing the PL as well as STM and SEM results of the two, can there be a more definite conclusion. Image scans (Figure 3.7d) reveal, these 2 peak Raman active areas are most pronounced at the crystal edges. This material demonstrates a sharp PL peak centered at 1.59 eV with an intensity of 2530 CCD counts which is closer to 1.57 eV observed in monolayer $MoSe_2$. However, another sharp PL peak can be observed at 1.53 eV closer to bilayer $MoSe_2$ (1.54 eV) [133]. AFM results of Figure 3.7e-f shows a step height measuring ~2.52 nm deviating from the expected 0.7 to 1 nm [134-136]. Also, the edges observed to be ~16 nm thick, much thicker than the basalt plain.

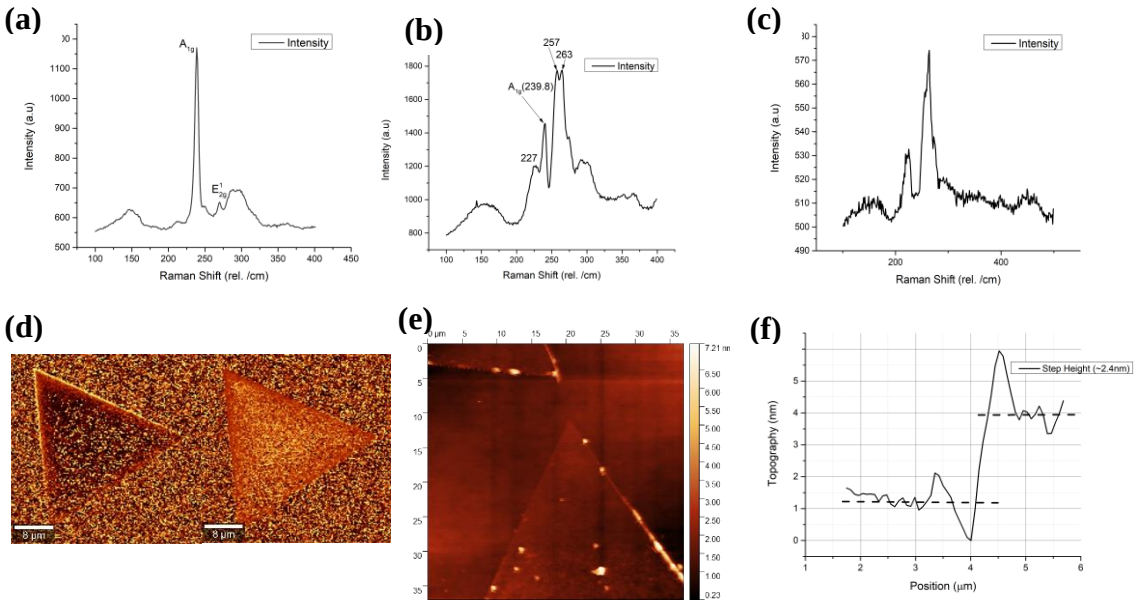


**Figure 3.7.** *Optical characterization of $MoSe_2$: (a) Raman spectra indicating monolayer 2H $MoSe_2$, (b) Raman spectra taken from a $MoSe_2$, with a star morphology, (c) Raman of $MoSe_2$ on grown on glass substrate, (d) Raman image scan with peak filtering, (e) AFM of $MoSe_2$ transferred onto $Si/SiO_2$ substrates, (f) Step height results extracted from the AFM image results.*

### 3.3. Transition Metal Carbides, (MXenes)

The MXene family of 2D materials encapsulates materials with a chemical composition of $M_{n+1}X_nT_x$, M representing a transition metal, X a carbon, nitrogen atom or a carbonitride and T a functional group (-O, -OH, or F). Gofotsi, otherwise known as the father of MXenes, exfoliated the first MXene, $T_3C_2T_x$ in 2011 [137] by selective etching of Al from $T_3AlC_2$ with HF. This is the most perverse method of MXene synthesis involving the etching out of the Al layer from Al-containing MAX phases [96, 137-140] using HF [137], $NH_4HF_2$ [141], LiF and HCl [142]. Selective etching of two Ga atoms from $Mo_2Ga_2C$ to produce $Mo_2CT_x$ has also been demonstrated as another alternative method of MXene synthesis [143]. Although CVD has proven a successful method for the synthesis of other 2D materials such as graphene and TMDCs, growth of MXenes via this means has yet to be fully explored. Xu et al. [144] used CVD to deposit large area and high quality $Mo_2C$ with a thickness of ~3 nm. Resistivity studies on 3.4 nm crystals indicated the decrease in resistivity as temperatures dropped from 300 to 50 K however, logarithmically rising as the temperature further falls beyond 50 K, just as observed in $Ti_3C_2T_x$ [141], suggestive of weak 2D localization effect.

Crystals with thickness greater than 3 nm demonstrated superconducting transitions and an electron mobility of 10 $cm^2 V^{-1} s^{-1}$ at 4 K and 10 K respectively. This intimates the absence of terminating functional groups as these are known to dull the material's electrical performance.

CVD offers so many advantages such as controlled deposition, repeatability and high-quality crystal growth the potential for mass synthesis. A trifle research attention is awarded to the growth of MXene by CVD despite the promising potential benefits. Inspired by this and the work by Xu et al., [144], this section focuses on the CVD method of synthesizing $Mo_2C$ and the possible extension to other MXenes such as $W_2C$ and $Ti_2C$.

### 3.3.1. CVD of $Mo_2C$

The synthesis set up for $Mo_2C$ closely resembles that of graphene in many aspects, the only differences being the tube diameter and the gas concentrations. The experimental setup is just as that illustrated in Figure 3.1 however, the tube used here is 2.54 cm (1 inch) in diameter. In the growth configuration, 3 solvent cleaned copper foils are placed above a molybdenum foil of the same dimension. Experiments are conducted at temperatures above 1083 °C, the melting point of Cu. To control crystal thickness and domain size either, growth time, the concentration of $CH_4$ or $H_2/N_2$ is varied while other parameters remain constant.

### 3.3.2. Observation and material characterization

Figure 3.8 illustrates the results of an experiment conducted at atmospheric pressure and temperature of 1100 °C, under gas flow of 75/25 sccm $H_2/N_2$. $CH_4$ representing the start and end of the experiment, was introduced at 1100 °C for 15minutes after which the lid of the reactor was opened, and the system cooled down naturally. Different crystal morphologies were observe including hexagonal, rectangular, circular, triangular as well as irregular shaped structures, similar to the observation by Xu et al., [144]. Figure 3.8a-c shows the optical images of the samples grown on Cu foil. Crystal distribution on the substrates was arbitrary, with dense areas (Figure 3.8a) as well as sparse areas (Figure 3.8b). Dark field images of the samples (Figure 3.8c) show the defined crystal boundaries. Figure 3.8d shows an image of the crystals transferred onto Au/Ti substrate. The grown samples were characterized by Raman spectroscopy and Atomic Force Microscopy (AFM).

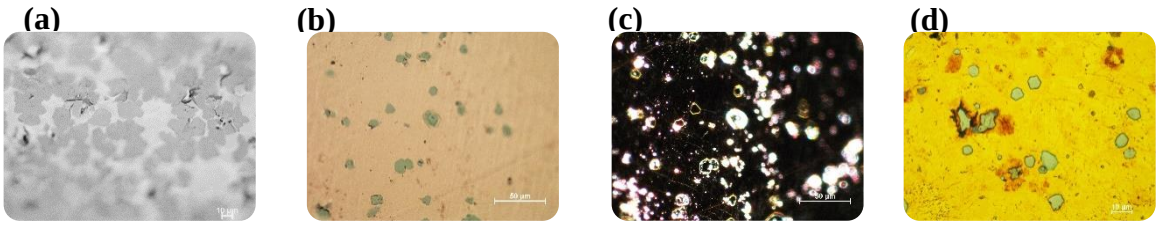


**Figure 3.8.** *Optical characterization of $Mo_2C$: (a) Densely packed MXene flakes on Cu substrates, (b) Image of as grown crystals with sparse distribution, (c) Dark field image of as grown MXene crystals and (d) $Mo_2C$ crystals transferred onto Ti/Au for SC application*

Theoretical calculations [145] suggest 36 vibrational modes in $Mo_2C$ amongst which 18 are Raman active. Experimental studies by Li, T., et al. [146] revealed 5 Raman active modes all of which are assigned either to $A_g$ or $B_{3g}$. In the Raman spectra shown in Figure 3.9a, the $B_{3g}$ peaks are located at frequencies 169.1 $cm^{-1}$ and 210.6 $cm^{-1}$ whereas the $A_g$ modes are found at 231.4 and 651.8 $cm^{-1}$, is close accord with the literature values [145, 146]. The $A_g$ mode at 192.1 $cm^{-1}$ and $B_{3g}$ mode at 169 $cm^{-1}$ are suggested to originate from the vibration of Mo atoms within the b–c plane whereas, the $A_g$ modes at 152.5 and 238.8 $cm^{-1}$ and $B_{3g}$ modes at 147.4 and 215.3 $cm^{-1}$ are generally the vibrations of Mo atoms outside the b–c plane [146]. One unassigned peak is observed at 140.3 and an unidentified peak at 70.68 $cm^{-1}$.

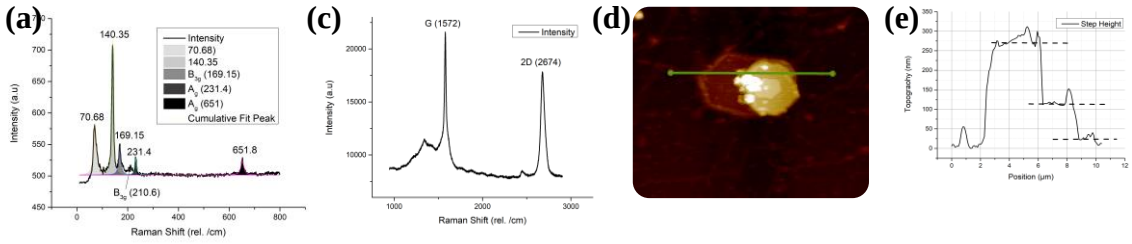


**Figure 3.9.** *Optical characterization of $Mo_2C$: (a) Raman spectra of $Mo_2C$, (b) Raman of the underlaying graphene, (c) AFM of $Mo_2C$ image showing topography of $Mo_2C$ crystal, (e) Sep height of $Mo_2C$*

Graphene was observed to grow beneath the $Mo_2C$, with a Raman spectrum shown in Figure 3.9b. The 2D/G Lorentz fitted peak ratio of this Raman spectra was calculated between 0.63 and 1; and the step height of ~4 nm to 16 nm, as measured by AFM, all indicative of multilayer graphene.

## 4. SUPERCAPACITOR BASED ON 2D MATERIALS

Two dimensional (2D) materials have drawn considerable research attention due to their extraordinary physiochemical properties and potential application in optoelectronic, sensing and energy storage technology etc. 2D materials being 1 or a few layers thick, means that their surface atoms are completely exposed, thus offering a large surface area for storage of electrolyte ions. Also, the edges of 2D thin films are made of broken bonds, thus rendering them more reactive as compared to the basal plane. Few layers 2D materials are held by weak Van der Waals forces, making it possible for the intercalation of electrolyte ions. Despite being atomically thick, their mechanical strength is considerably high, opening doors for potential applications in flexible energy storage [94].

### 4.1. Graphene Supercapacitors

Graphene is a single layer of all-$sp^2$-hybridized carbon atoms densely packed in a hexagonal or Benzene-ring structure [66]. Graphene, a pioneer 2-dimensional material, was successfully exfoliated by Novoselov, K.S., et al. [147] and has since opened many doors for applications in a myriad field due to its extraordinary properties. Among these promising areas is energy storage in SCs applications. A single layer of graphene possesses a theoretical highly tunable surface area of reaching 2675 $m^2 g^{-1}$ which if exhaustively utilized can store charge with a specific capacitance of ~21 to 28 $\mu F\ cm^{-2}$ [92, 93], which is just about 550 F $g^{-1}$ of gravimetric capacitance [66]. Graphene (also highly conductive to electricity, with a carrier mobility of 200,000 $cm^2v^{-1}s^{-1}$ at an electron density of ~$2x10^{11}$ $cm^{-2}$ [148]) possesses the potential to boost the power density of an SC, which is contingent in an inverse proportionality to the electrode's internal resistance. Its high mechanical strength – Young's Modulus of $E \approx 1TPa$ [149], makes its use in flexible energy storage systems a feasible reality as well as the ability to assemble them into free-standing films with robust mechanical stability. Graphene is chemically stable [66, 150], meaning that different electrolytes can be used without fear of decomposing the active material, thus ensuring a longer life for the SC.

For supercapacitor application, graphene is considered one of the most promising materials. However unfortunately, little success has been achieved exploiting the benefits offered by graphene in this field. This is accounted for by serious agglomeration (resulting from the inter-planar $\pi$-$\pi$ interaction and van der Waals forces) occurring either during the growth or the application stage, making it cumbersome for electrolyte ions to intercalate in

graphene layers, resulting in a lower capacitance value than anticipated [66]. 8 layers of graphene obtained by repeated dry transfer of CVD grown graphene achieved a specific capacitance of 62.8 μF $cm^{-2}$, corresponding to 36.8 F $cm^{-3}$ in PVA/ $H_2SO_4$ hydrogel electrolyte. This was boasted by the ionogel electrolyte to 147 F $cm^{-3}$ at a scan rate of 10 V $s^{-1}$ and a power density of 1860 W $cm^{-3}$ at an energy density of 23 mW $cm^{-3}$ [79]. Another study by Zang, X., et al. [151], in button cell SCs, using 1-butyl-3-methylimidazolium tetrafluoroborate (BMIM-PF4) obtained specific capacitances of 100 μF $cm^{-2}$ and 290 μF $cm^{-2}$ for 1 layer and 10 layers of graphene respectively at a scan rate of 10 mV $s^{-1}$. Graphene prepared by other methods such as by exfoliation of graphitic oxide was able to attain a capacitance of 117 F $g^{-1}$ using 1M $H_2SO_4$ [152]. A few attempts have been made to combat restacking of graphene sheets by introduction of spacers. The most pervasively investigated spacers are in the form of carbonaceous (e.g. carbon quantum dots and Carbon Nanotubes, CNT), metals such as Pb, Pt [153] and Au, metal oxides and pseudocapacitive materials amongst which are metals oxides and hydroxides as well as conductive polymers [66, 154, 155]. Intercalators alleviate the restacking issue of Graphene sheets boasting its practical capacitance value to ~300 F $g^{-1}$ [156], which is still just barely above half of the expected. Even though spacers help increase active area of the electrode, they might also have side effects like weakening the conductivity of the pristine graphene.

Inspired by Zang, X., et al. [151], herein, we explore the performance of different layers of graphene grown by CVD on Copper substrate and transferred onto a Titanium-Gold (Ti/Au) coated glass substrate. Although CVD graphene is scarcely used for SC fabrication due to high production cost (with preference given to reduction of graphene oxide), it nevertheless has few defect densities, a uniform coverage and continuous or large crystal domains [156]. We are of the opinion that by sequential transfer of one layer of Graphene onto another to form multiple layers, the agglomeration could be mitigated.

### 4.1.1. Fabrication of sandwich-type graphene supercapacitors

To test a materials performance, a 3 electrode configured cell or a test cell can be used [157]. Herein, we have constructed our own supercapacitors (test cells) based on the description by Conway [1]. Figure 4.1a shows the framework of our supercapacitors which is made up of a metal coated glass substrate onto which the active material is transferred,

forming a single electrode. The two electrodes are assembled with an electrolyte and impregnated separator place in sandwich to these electrodes. The fabrication of the devices can be divided into 3 steps: metal coating of the current collectors; transfer of the active material, device assembly and encapsulation (Figure 4.1b).

#### *4.1.1.1.Deposition of current collectors*

Lamella glass slides are chosen as electrodesubstrates due to their affordability as compared to Si wafers. The glass substrates are ultrasonicated in a bath of acetone, isopropanol (IPA) and deionized (DI) water for a 5 mins duration each. The clean samples are then coated with 10 nm of Titanium as the binder and 90 nm of Gold using NVTH-350 thermal evaporator.

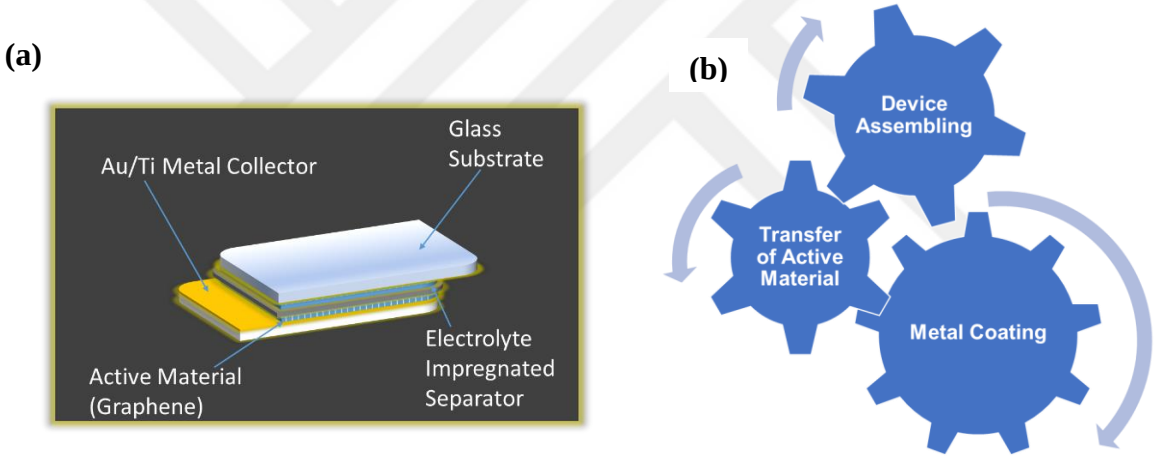


**Figure 4.1.** *Supercapacitor's construct: (a) schematic of an EDLC, (b) fabrication process flow*

#### *4.1.1.2.Material transfer*

Graphene is grown on Cu substrates, so it is required to be transferred onto a suitable substrate for SC application. This can be achieved either through dry by use of pressure sensitive adhesive films [158] or wet etching [159] techniques. All our materials are transferred by wet etching as illustrated in Figure 4.2.

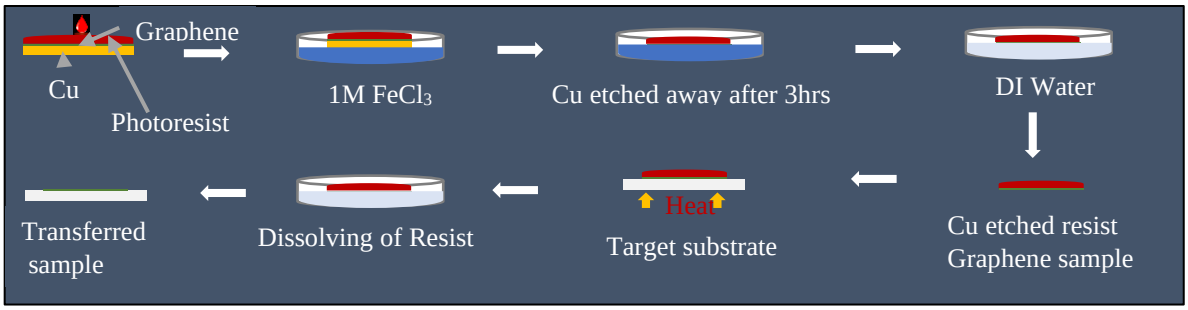


**Figure 4.2.** *Schematic illustration of graphene transfer procedure.*

The sample to be transferred is first drop casted with photoresist (AZ5214) and at atmospheric pressure in an oven set at a temperature of 70 °C for a duration of at least 12 hrs. The sample is then removed and put in a 1M solution of $FeCl_3$ for 3 hours to etch away the Cu substrate. With the Cu etched away, the remaining resist-graphene film is carefully removed using Teflon tweezers (to avoid corrosion of metallic tweezers) and placed in DI water for 10 minutes, and this process is repeated 3 times. This is to make sure that all the etchant is thoroughly removed. The resist-graphene film is then dried with $N_2$ and placed onto the target substrate with the graphene side facing down. The substrate is now baked in a hotplate at 70 °C for 5 to 10 mins until the resist completely sticks to the substrate. The sample is then immersed into a solution of acetone to dissolve the photoresist. With the resist dissolved, the sample is removed, cleaned with acetone, followed by IPA and finally dried with $N_2$ and the transfer is complete.

#### *4.1.1.3.Device assembling*

The devices are assembled as shown in Figure 4.1a. The separator (microfiber whipper with a thickness of 66 μm) is placed on the substrate covering the area occupied by graphene. Two three drops of electrolyte solution (in this case 1M $Na_2SO_4$) applied to the separator. The other electrode is then placed on top of the separator slide to the side leaving the area not covered by graphene to serve as the contacts of the SC.

Encapsulation of the devices is of paramount importance since otherwise the electrolyte evaporates away giving faulty results for long duration measurements. This is achieved by covering the sample with polyethylene terephthalate, PET, while only exposing

the contacts. However, the electrolyte dries during lamination, so it must be reintroduced using a syringe, and using an insulating tape to cover the hole created.

### 4.1.2. Device characterization

Performance of our SCs is measured using the GAMRY potentiostat arranged in a two-electrode configuration (working and working sense connected to one electrode and the counter and reference electrodes connected to the other). In order to measure the capacitance, the durability and the internal resistance of our SCs, we performed cyclic voltammetry (CV), electrochemical impedance spectroscopy (EIS) and constant current charge discharge analysis (CCCD).

#### *4.1.2.1. Results and discussion*

SCs in this work are constructed with a 1.5 x 1.5 dimension. We have constructed SCs with different layers of graphene. The graphene used for our devices has a Raman peak that suggest multilayer and a thickness of about 4 nm as measured by AFM. The growth time of this graphene is 5mins with other parameters remaining the same. However, we have adopted the "1 Layer" term to represent each layer of graphene grown with this recipe. "Multiple layers", are obtained by repeated transfer of one layer onto another. The performance of these devices is analyzed by taking CV, EIS and CCCD.

#### *4.1.2.2. Cyclic voltammetry, CV*

Cyclic voltammetry is a technique where current developed in an electrochemical cell is measured under conditions where the potential difference exceed that predicted by the Nernst Equation. This is usually achieved by cycling the potential of the working electrode, while measuring the resulting current.

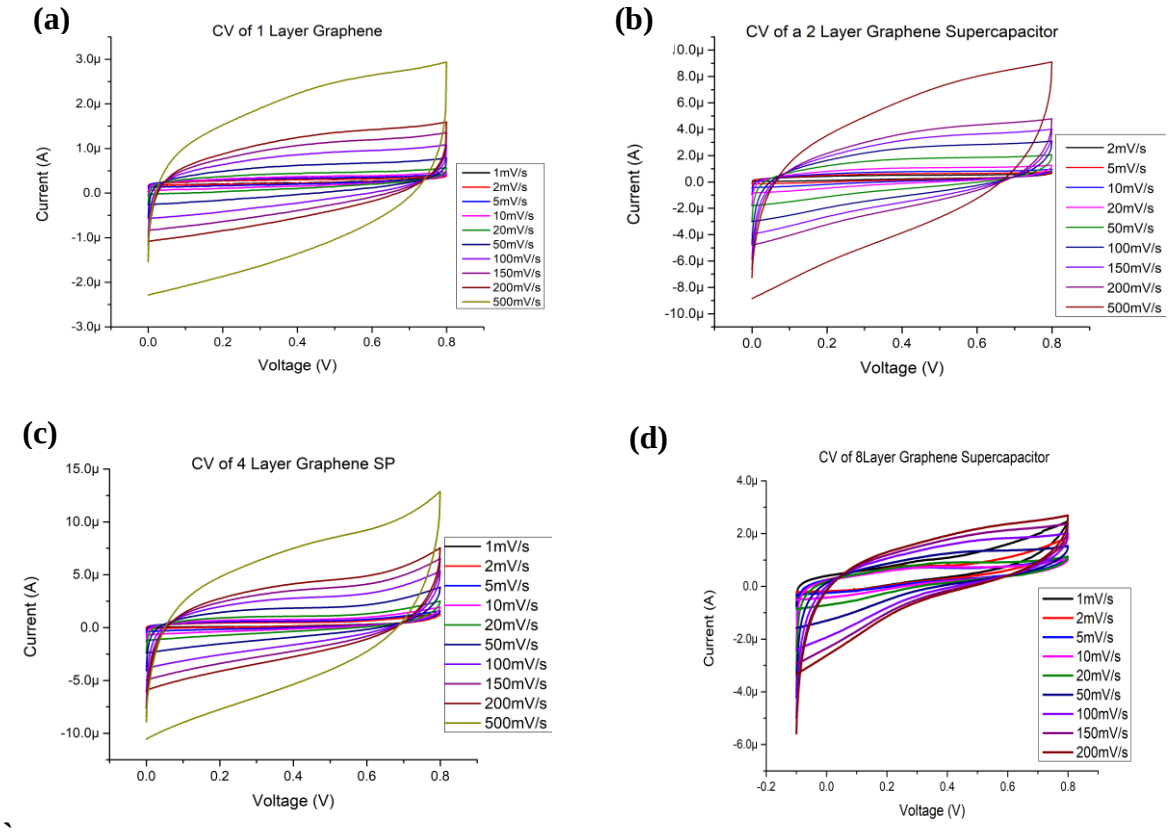


**Figure 4.3.** *CV of different layers of Graphene: (a) 1layer graphene (~0.63 nm), (b) 2-layer graphene (~2 x 0.63 nm), (c) 4-layer (~4 x 0.63nm), (d) 8 layers of graphene (~8 x 0.63 nm).*

Different scan rates offer different capacitances, with the highest measured at small scan rates. We have performed CV at scan rates of 1, 2, 5, 10, 20, 50, 100, 200 and 500 mV $s^{-1}$, the results of which are shown in Figure 4.3. A voltage window of 0 - 0.8 V was used; this was determined by the electrolytes (1M $Na_2SO_4$) operation voltage range. Figure 4.3 shows the CVs of 1, 2, 4 and 8 layers of graphene each having a rectangular outline indicative of infinitesimal pseudocapacitive influences. The area of the CV curve also increases as the scan rate is increased, concordant to our expectations. Capacitances can be calculated from the CV using E.4.1 [160], where S is the area between the CV curve, v the scan rate and V the voltage window, if the full width of the CV is utilized. The area S is considered from the part of the CV which is as rectangular as possible (Figure 4.4a).

$$C = \frac{\int_{V_1}^{V_2} i\, dV}{2v|V_2 - V_1|} = \frac{S}{2vV} \tag{4.1}$$

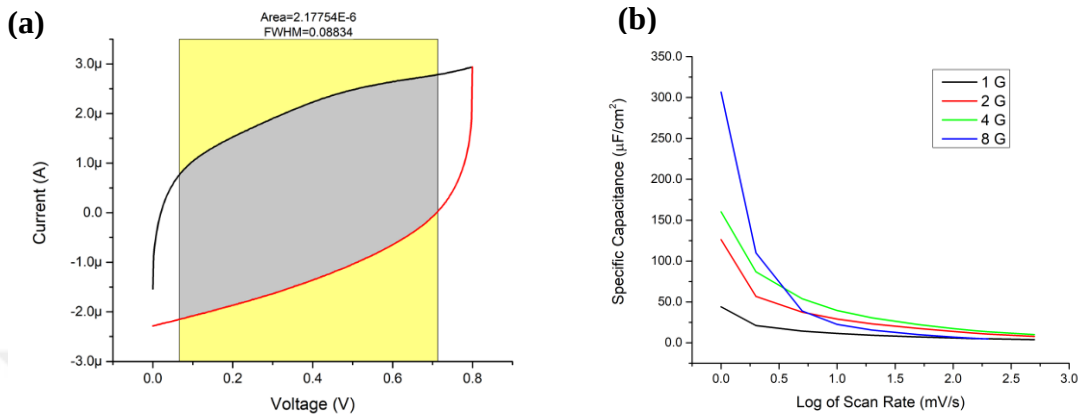


**Figure 4.4.** *Capacitance: (a) CV demonstrating area in capacitance calculation, (b) graph of specific capacitance vs scan rate*

Capacitance calculated using E.4.1, are normalized by the area of one (average area of the two electrodes since they are not perfectly symmetric) electrode to obtain a specific capacitance [161]. The capacitance of '1 layer' graphene decreases from a value of ~44 μF $cm^{-2}$ at a scan rate of 1 $mVs^{-1}$ to ~4 μF $cm^{-2}$ at a scan rate of 500 mV $s^{-1}$, with a rate stability of 9%. The volumetric capacitance measures up to 697 F $cm^{-3}$, and gravimetric capacitance of 308 F $g^{-1}$ giving an energy density of 27.38 Wh $kg^{-1}$ at a scan rate of 1 mV $s^{-1}$. The capacitance of '2 layers' is measured as 126 μF $cm^{-2}$ at a scan rate of 1 mV $s^{-1}$ which is almost 3 times compared to that of the '1 layer' at the same scan rate. This can be explained by assuming that the electrolyte now has access to 3 surfaces since the side attached to the current collector might be inaccessible. The capacitances for '4 and 8 layers', are 160 and ~306 μF $cm^{-2}$ at 1 mV $s^{-1}$ respectively. The capacitance of '8 layers' graphene is almost double that of the '4 layer' suggesting almost negligible layer agglomeration; however, this is not the case when the capacitance of '2 layer' and '4' layer are compared. This value is only about a 27% increase in capacitance as opposed to the expected 100%. This might be due to inconsistencies occurring during material transfer as well as layer restacking. Interestingly, the gravimetric capacitance is observed to increase from 307 F $g^{-1}$ to 441 F $g^{-1}$ and decreases to 280 F $g^{-1}$ and 268 F $g^{-1}$, with each doubling of the electrode material thickness (i.e. 1, 2, 4 & 8).

### *4.1.2.3.Electrochemical impedance spectroscopy, EIS*

The frequency response of our SCs were evaluated at a frequency range of 10 mHz to 1 MHz. Figure 4.5a-b shows the Nyquist and the Bode plots of SCs, fabricated with '4 layers' of graphene.

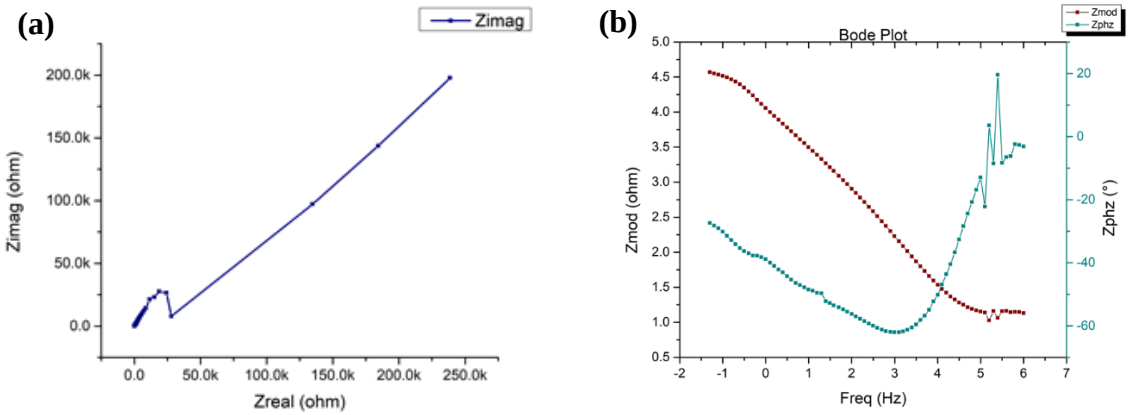


**Figure 4.5.** *Frequency response of 4L graphene: (a) Nyquist plot, (b) Bode plot*

At very high frequencies, the resistance recorded in the Nyquist curve approximates to the equivalent series resistance, ESR, of the SC and can be obtained by extrapolation x-intercept of the curve as explained in section 2.2.1.1 (see E.2.3). ~14 Ω and ~10 Ω of ESR is measured for '4 layer' and '2 layer' graphene respectively. The power density for the 2 layer graphene was measured as 12.4 kW $g^{-1}$. In the bode plot, the phase of the SC lies mostly in the $4^{th}$ quadrant, indicative of purely capacitive behavior. The magnitude of the impedance decreases almost linearly as the log of the frequency increases.

### *4.1.2.4.Constant current charge discharge*

From charging and discharging an SC, we can obtain information patterning capacitance at varied current densities and its capacitance retention capability. Capacitance can be calculated from the slop of the SCs discharge curve by using E.4.2 [162], with I, being either the current density (to give specific capacitance) or discharge current (for simple capacitance).

$$C = \frac{I}{dv/dt} \tag{4.2}$$

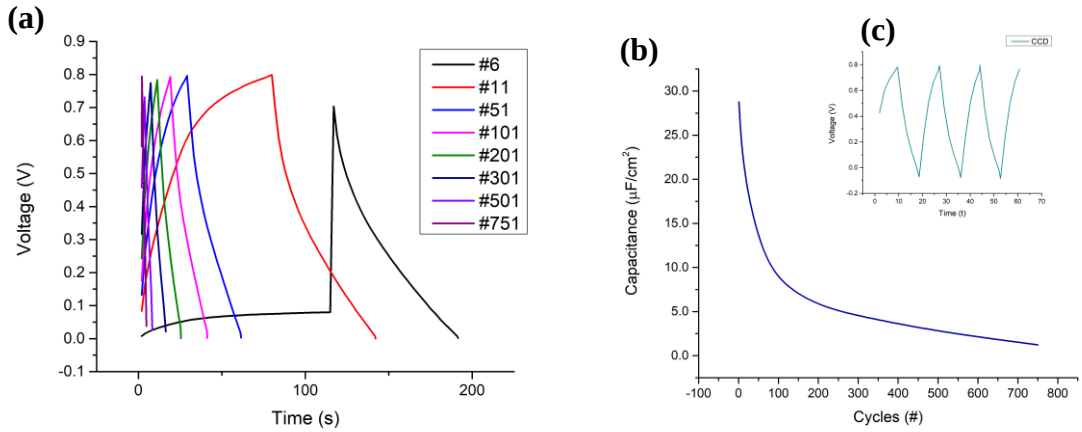


**Figure 4.6.** *CCD results of an SC based on graphene: (a) Charge discharge curves after a random number of cycles, (b) Curve of capacitance (calculated from the discharge curve) vs. cycle number, indicating the capacitors retention capability, (c) Continuous CCCD for the first four charge discharge cycles.*

Charge discharge of the SCs below 10 times shows stability of the capacitance value as depicted in Figure 4.6a and c. However, as the number increases, the capacitance drops markedly as shown in Figure 4.6b. This is incongruous with our expectations; however, an explanation can be found in the fact that our SCs were not encapsulated and the electrolyte evaporated with time.

## 4.2. Graphene-MXene Hybrid Supercapacitor.

The word MXene refers to a family of 2D materials with a chemical composition of $M_{n+1}X_nT_x$, where M represents a transition metal, X a carbon, nitrogen atom or a carbonitride and T a functional group (-O, -OH, or F). MXenes ($T_3C_2T_x$) were first exfoliated in 2011 by Gogotsi [137], via selective etching of Al from $T_3AlC_2$ with HF.

With a morphology similar to graphene, MXenes as a promising materials for 2D electrode material, are endowed with a decent intrinsic electronic conductivity, hydrophilicity, high ductility and excellent mechanical and chemical stability [94-96]. MXenes also possess large interlayer spacings which are conducive to ionic intercalation [77]. For example, freestanding $Ti_3C_2$ films with intercalated water, prepared by etching in LiF and HCl, exhibited a volumetric capacitance of 900 F $cm^{-3}$ at 20 mV $s^{-1}$ in 1M $Na_2SO_4$. The gravimetric capacitance was measured at 245 F $g^{-1}$ at 2 mV $s^{-1}$, and magnificent cycle stability (100% capacitance retention after 10000 cycles) [142].

2D transition metal carbides/nitrites are generally prepared by selectively etching the 'A' atomic layer from the bulk MAX phases [77]. MXenes prepared by this means, are usually terminated by functional groups (-O, -OH, -F), which weaken their electrical properties [69]. CVD grown MXenes are not terminated by functional groups; thus, they are expected to demonstrate higher conductivity. This work is motivated by this fact and is aimed at making SCs higher power densities. However, CVD growth of $Mo_2C$ is accompanied by an underlying layer of few layer graphene. Graphene is also a good electrode material and by synergizing the best properties of each material in a composite hybrid SC, we can hope to boost the SC's performance. Unfortunate it is difficult to extract the performance contribution of just $Mo_2C$ for comparative analyses. Notwithstanding this, devices have been fabricated by hybridizing the graphene and MXene in a composite arrangement.

The SC fabrication procedure are analogous to those illustrated in Figure 4.1, with the only difference being in the $Mo_2C$'s transfer process. Glass substrates are first coated with the current collector (Ti/Au), followed by transfer of the active material (here $Mo_2C$), placement of electrolyte impregnated separator, alignment of the electrodes and encapsulation.

### 4.2.1. Transfer of MXenes.

Figure 4.2 illustrates the transfer procedure that is used for graphene which is more or less the same as $Mo_2C$ except for some few exceptions. First, $Mo_2C$ which is grown on a Cu/Mo substrate, is drop coated with photoresist (AZ5214) and baked at 70 °C for at least 12hrs. The sample is then removed and immersed into a solution of 3M $FeCl_3$ to etch away the alloy substrate. It takes about 9 hrs. to dissolve the metallic substrate after which the resist film is removed and cleaned by successively immersing in three DI water filled petri dishes for 10 minutes each. Assuming the metal etchant is removed the film is then placed onto the target substrate and baked at 70 °C until the film adheres to the substrate. The resist is then dissolved in acetone and the transfer is done.

### 4.2.2. Characterization and performance evaluation

The SCs are assembled in a similar manner as explained in section 4.1.1.3. Performance analysis was done using a Gamry potentiostat in a two-electrode configuration. CV, EIS and CCCD results are evaluated to obtain information on capacitance, ESR and device durability.

### *4.2.2.1.Cyclic voltammetry, CV*

In a voltage window of 0 – 0.8 V, CV of the device is conducted at different scan rates as shown in Figure 4.7a. The symmetry and the fairly rectangular nature of the CVs is telling of negligible or no pseudocapacitive influences. The specific capacitance drops from a value of ~0.67 mF $cm^{-2}$ at a scan rate of 1 mV $s^{-1}$ to 22 µF $cm^{-2}$ at 500 mV $s^{-1}$, demonstrating a rate stability of 3.3% at 500 mV $s^{-1}$.

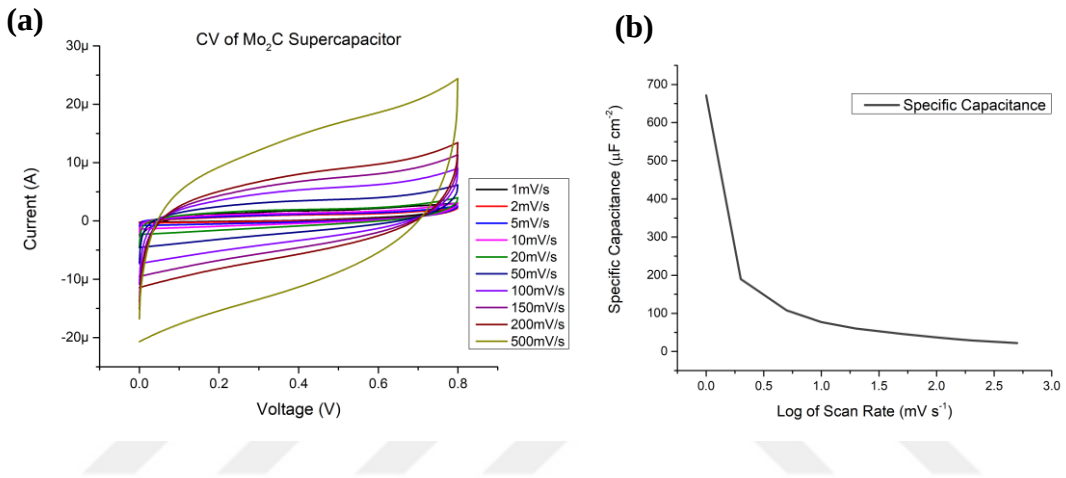


**Figure 4.7.** *CV results: (a) CV at different scan rates, (b) specific capacitance obtained from different scans*

### *4.2.2.2.Electrochemical Impedance Spectroscopy, EIS*

The results obtained from EIS is represented by a Nyquist and a Bode plot as shown by Figure 4.8. The ESR measure from the complex-impedance-plane plot is 2.8 Ω, extrapolated from the high frequency region of the curve. Unfortunately, the locus of points could not be observed therefore, information of the leakage current cannot be extracted suggesting a need for a more complex model. This might be related to the drying of the electrolyte as EIS scans usually last for hours and our devices are inconspicuous. However, the imaginary part of the modeling circuit, tends to ∞ as the frequency approaches 0.

The magnitude of the impedance decreases as the frequency increases and the ESR can be estimated by extrapolating the resistance value at infinite frequency. The phase angle tends to 0 ° at high frequencies indicative of the influence of the leading ESR.

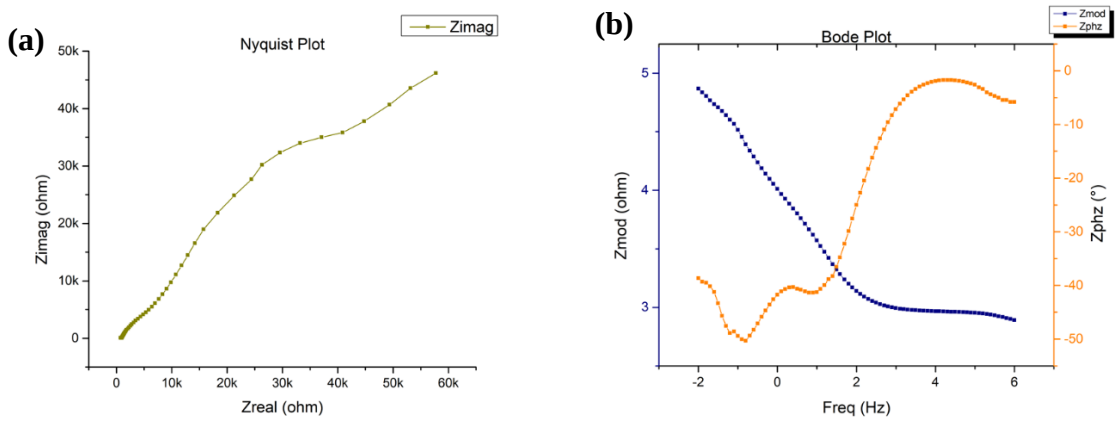


**Figure 4.8**. *EIS of $Mo_2C$. (a). Nyquist plot. (b). Bode plot*

### *4.2.2.3.Constant current charge discharge, CCCD*

CCD is measured at a constant current of 1.5 µA. Capacitance value decreases exponentially from 230 µF $cm^{-2}$ at earlier cycles to 9.8 µF $cm^{-2}$ at 750 charge discharge cycles with a capacitance retention of only 4.3 % after 750 charge discharge cycles. This is probably because of the absence of encapsulation resulting in evaporation of the electrolyte solvent leaving only salt residues.

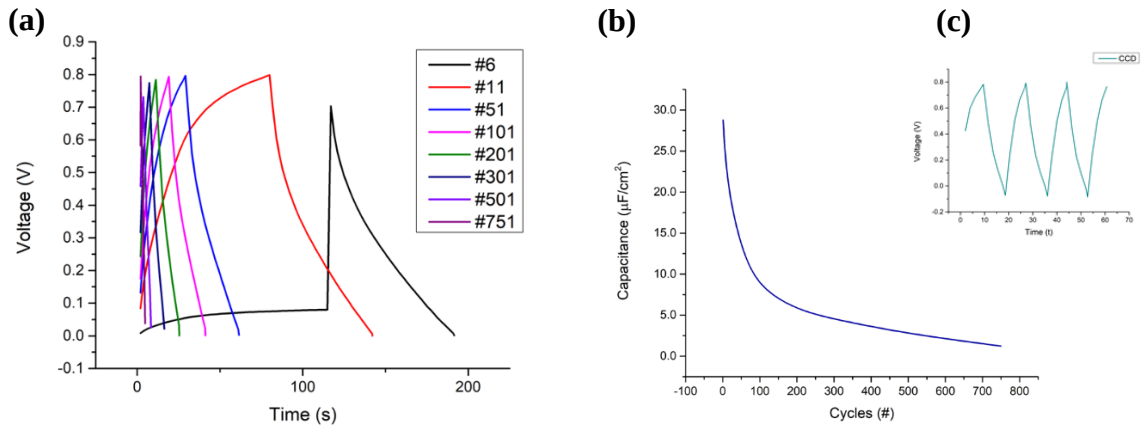


**Figure 4.9.** *CCD of $Mo_2C$ based SC: (a) Charge discharge curves after a random number of cycles, (b) Curve of capacitance (calculated from the discharge curve) vs. cycle number, indicating the capacitors retention capability, (c) Continuous CCCD for the first four charge discharge cycles.*

### 4.2.3. Prospects for better performing SCs

The restacking of 2D layers during growth or device fabrication is a serious issue that stems their SCs from exercising superior performances. The benefits offered by 2D materials

cannot be exploited if this issue perpetuates. Direct deposition of the active material on the metal collector eliminates the desire for rather expensive binders. Though a tedious approach, repetitive transfer of the 2D layers to form multilayer can help alleviate agglomeration problems.

Individual materials exhibiting higher energy storage capabilities like TMOs are generally plagued by high resistivity and slow charging issues. Albeit high volumetric capacitances, MXenes on the other hand exhibit low gravimetric capacitances due to their low surface area (30 $m^2 g^{-1}$) [69]. Hybridizing MXenes with high surface area materials, for e.g. TMO/TMH or TMDCs could produce a synergy of their properties boasting the device's overall performance.

### 4.3. Supercapacitors Based on TMDCs

2D transition metal dichalcogenides have also drawn considerable research attention in many applications including energy storage in SCs. They are endowed with a high surface area originating from their sheet-like morphology. They exhibit variable oxidation states (e.g. +2 to +6 in $MoS_2$), conducive for pseudo active, increasing their energy storage potential [163, 164]. Dangling bonds present in their edge sites favor high electrochemical activity, thus boasting energy storage capability [165]. The ability of TMDCs to exist in different phases such as the metallic 1T [166] and the semiconducting 2H phases, brings about additional benefits in energy storage such as increase conductivity and voltage operation window [94].

Within the constraints of time, SCs based on TMDCs were not realized, as much of this went in optimizing their growth procedure. This section has been tabled for future studies, the plan being to construct and evaluate the performance of hybrid micro supercapacitor (planner) based on MXenes and TMDCs.

### 4.4. Discussion and conclusion

Colossal research efforts have been dedicated to developing novel methods for processing graphene-based materials such as reduction of spin-coated GO [167], layer-by-layer doping of CVD grown graphene [168], wet chemical etching (based on interfacial self-assembly) [169], vacuum filtration [170] etc. However, due to layer agglomeration which greatly reduces the available surface area for charge storage as well as hinder electrolyte

diffusion, they have been met with inferior constraint below 100 F $g^{-1}$. At a current density of 0.3 A $g^{-1}$, graphene based SCs produce a capacitance of 57 F $g^{-1}$ [171]. Previous studies using graphene electrodes, have demonstrated capacitances of 135 F $g^{-1}$ and 99 F $g^{-1}$ at a discharge current of 10 mA (i.e. 100 F $g^{-1}$ and 99 F $g^{-1}$ at 20 mV $s^{-1}$) and 75 F $g^{-1}$ in aqueous (KOH), organic ($TEABF_4$/AN), and ionic liquid ($PYR_{14}TFSI$) electrolytes, respectively [152, 157]. In this work we observed the highest capacitance of 441 F $g^{-1}$ at a scan rate of 1 mV $s^{-1}$ using a neutral electrolyte ($Na_2SO_4$) and a graphene electrode of ~1.26 nm in thickness. This value is almost comparable to the predicted capacitance of a single sheet of graphene electrode of 550 F $g^{-1}$ [66, 92, 93]. Although this value has decreased as the mass loading is increased, a capacitance of 268 F $g^{-1}$ is obtained at quadruple the initial mass loading at the same scan rate (1 mV $s^{-1}$).

With the restacking of graphene sheets being tackled at least partially, the gravimetric specific capacitance of graphene films continues to improve. For example, using chemically modified graphene and polyaniline nanofiber as a composite electrode material, Zhang et al. [172], were able to obtain a capacitance of 480 F $g^{-1}$ at a current density of 0.1 A $g^{-1}$. Despite efforts to reduce agglomeration, capacitance performance could only be increased this much. In our study, although tedious, transferring CVD graphene one layer at a time directly to the metal collector, has yielded two main benefits. The agglomeration problem was considerably tackled as was indicated by the high capacitance of 441 F $g^{-1}$. The desire for binders was also eliminated as the materials were directly transferred onto the current collectors, thus helping to reduce the overall fabrication cost.

To surmount the agglomeration problems that occur in 2D materials-based SC systems, sequentially stacking of different layered materials is also another promising alternative. In this dissertation, using a graphene – $Mo_2C$ composite we achieved a specific capacitance of 0.67 mF $cm^{-2}$, which is about 2 folds higher than in the case of 5.04 nm (about 16 layers) thick graphene SC and almost 15 times greater than the case of using 0.63 nm (i.e. bilayer graphene) thick graphene. This shows that by using a hybrid configuration, the specific capacitance of an SC can be significantly improved, and our hybrid structure can be modified to obtain high performance parameters. This can be done in several ways such as: incorporating pseudo active materials like TMDCs in the hybrid structure which can increase the capacitance performance; fabricating an in plane micro supercapacitor could also boast

the power density due to small inter-electrode spacing and using monolayer graphene and MXene as base material, stacking them in a alternating array could greatly reduce agglomeration occurring in the individual materials. Nature has also provided us with so many hints and if some of them like the arrangement of veins in a plant leaf (which is designed for maximum sunlight absorption) can be adopted in our material, or electrode design, it might be possible to increase the active area for charge storage, thus increasing the capacitance.

**REFERENCES**


[1]. Conway, B.E., *Electrochemical Supercapacitors Scientific Fundamentals and Technological Applications*. 1 ed, ed. 1. 1999: Springer US.

[2]. Dummer, G.W.A., *Electronic inventions and discoveries : electronics from its earliest beginnings to the present day*. 1997, Institute of Physics Pub.: Bristol, U.K. ;.

[3]. Ho, J., T.R. Jow, and S. Boggs, *Historical introduction to capacitor technology*. IEEE Electrical Insulation Magazine, 2010. **26**(1): p. 20-25.

[4]. Cohen, I.B., *Benjamin Franklin's Experiments: A New Edition of Franklin's Experiments and Observations on Electricity*. Journal of Philosophy, 1941. **38**(26): p. 717-718.

[5]. *On the experiment of the dissectible condenser*. Am. J. Phys., 1944. **12**: p. 324.

[6]. Fitzgerald, D.G., *Improvements in electrical condensers or accumulators*, in *British Patent*. 1876.

[7]. Niwa, S. and Y. Taketani, *Development of new series of aluminium solid capacitors with organic semiconductive electrolyte (OS-CON)*. Journal of Power Sources, 1996. **60**(2): p. 165-171.

[8]. Qin, S., S. Ma, and S.A. Boggs. *The mechanism of clearing in metalized film capacitors*. in *2012 IEEE International Symposium on Electrical Insulation*. 2012.

[9]. McLean, D.A., *Metallized Paper for Capacitors.* Proceedings of the IRE, 1950. **38**(9): p. 1010-1014.

[10]. Cozens, J., *Development of Plastic Dielectric Capacitors.* IRE Transactions on Component Parts, 1959. **6**(2): p. 114-118.

[11]. Becker, H.I., *Low Voltage Electrolytic Capacitor*. United States Patent Office, 1957.

[12]. Rightmire, R.A., *Electrical Energy Storage Apparatus.* United States Patent Office, 1966.

[13]. Conway, B.E., *Transition from "Supercapacitor"to "Battery" Behaviorin Electrochemical EnergyStorage.* ELECTROCHEMICAL SCIENCE AND TECHNOLOGY, 1991. **138**(6, 1539-1548).

[14]. Wagner, L., *Chapter 27 - Overview of Energy Storage Technologies*, in *Future Energy (Second Edition)*, T.M. Letcher, Editor. 2014, Elsevier: Boston. p. 613-631.

[15]. Huggins, R., *Energy Storage*. 1 ed. 2010: Springer US. XXVIII, 406.

[16]. Allan H. Robbins, W.C.M., *Circuit Analysis. Theory and Practice*. 5 ed. 2012.

[17]. KEMET. *Introduction to Capacitor Technologies*. 2013; Available from: http://www.kemet.com/Lists/TechnicalArticles/Attachments/6/What%20is%20a%20Capacitor.pdf.

[18]. Illinois, U.o. *Capacitance and Dielectrics*. 2019; Available from: https://www.coursehero.com/file/11597700/phys212-ch5-Capacitance/.

[19]. Kong, L.B., *Nanomaterial for Supercapacitors*. 2017: Library of Congress Cataloging-in-Publication Data.

[20]. Marts, J.D., *Enhanced physics-based reduced-order model of non-faradaic electrical double-layer capacitor dynamics (Order No. 10808681).* 2018.

[21]. Buchla, T.L.F.D.L., *Electronics Fundamentals Circuits, Devices and Applications*. 8th ed. 2014: Pearson Education Limited.

[22]. Burke, A., *Ultracapacitors: why, how, and where is the technology*. Journal of Power Sources, 2000. **91**(1): p. 37-50.

[23]. Kötz, R. and M. Carlen, *Principles and applications of electrochemical capacitors.* Electrochimica Acta, 2000. **45**(15): p. 2483-2498.

[24]. Zhang, L.L. and X.S. Zhao, *Carbon-based materials as supercapacitor electrodes.* Chemical Society Reviews, 2009. **38**(9): p. 2520-2531.

[25]. Szubzda, B., et al., *Polymer membranes as separators for supercapacitors.* Applied Physics A, 2014. **117**(4): p. 1801-1809.

[26]. Bispo-Fonseca, I., et al., *Possible improvements in making carbon electrodes for organic supercapacitors.* Journal of Power Sources, 1999. **79**(2): p. 238-241.

[27]. Schneuwly, A. and R. Gallay, *Properties and Applications of Supercapacitors From the State-of-the-art to Future Trends*. 2000.

[28]. Bittner, A.M., et al., *Ageing of electrochemical double layer capacitors.* Journal of Power Sources, 2012. **203**: p. 262-273.

[29]. Staiti, P., M. Minutoli, and F. Lufrano, *All solid electric double layer capacitors based on Nafion ionomer*. Electrochimica Acta, 2002. **47**(17): p. 2795-2800.

[30]. Zhang, S., Y. Li, and N. Pan, *Graphene based supercapacitor fabricated by vacuum filtration deposition.* Journal of Power Sources, 2012. **206**: p. 476-482.

[31]. Lekakou, C., et al., *Carbon-Based Fibrous EDLC Capacitors and Supercapacitors.* Journal of Nanotechnology, 2011. **2011**: p. 8.

[32]. Halper, M.S. and J.C. Ellenbogen, *Supercapacitors : A Brief Overview.* Semantic Scholar, 2006.

[33]. Raza, W., et al., *Recent advancements in supercapacitor technology.* Nano Energy, 2018. **52**: p. 441-473.

[34]. Kong, L.B., *Nanomaterials for Supercapacitors*. 2017, CRC Press.

[35]. Hui Xiaa, z., Ying Shirley Mengb,*, Guoliang Yuana, Chong Cuia and Li Luc,z, *A Symmetric RuO2/RuO2 Supercapacitor Operating at 1.6 V by Using a Neutral Aqueous Electrolyte.* ECS - The Electrochemical Society, 2012.

[36]. Snook, G.A., P. Kao, and A.S. Best, *Conducting-polymer-based supercapacitor devices and electrodes.* Journal of Power Sources, 2011. **196**(1): p. 1-12.

[37]. Zhang, Y., et al., *Progress of electrochemical capacitor electrode materials: A review.* International Journal of Hydrogen Energy, 2009. **34**(11): p. 4889-4899.

[38]. Mastragostino, M., C. Arbizzani, and F. Soavi, *Conducting polymers as electrode materials in supercapacitors.* Solid State Ionics, 2002. **148**(3): p. 493-498.

[39]. Arbizzani, C., M. Mastragostino, and F. Soavi, *New trends in electrochemical supercapacitors.* Journal of Power Sources, 2001. **100**(1): p. 164-170.

[40]. Peng, C., et al., *Carbon nanotube and conducting polymer composites for supercapacitors.* Progress in Natural Science, 2008. **18**(7): p. 777-788.

[41]. Frackowiak, E., et al., *Supercapacitors based on conducting polymers/nanotubes composites.* Journal of Power Sources, 2006. **153**(2): p. 413-418.

[42]. Zuo, W., et al., *Battery-Supercapacitor Hybrid Devices: Recent Progress and Future Prospects.* Advanced science (Weinheim, Baden-Wurttemberg, Germany), 2017. **4**(7): p. 1600539-1600539.

[43]. Huiqiao Li, L.C., and Yongyao Xia, *A Hybrid Electrochemical Supercapacitor Based on a 5 V Li-Ion Battery Cathode and Active Carbon.* Electrochemical and Solid-State Letters, 2005.

[44]. Wang, X., et al., *Pseudocapacitance of MXene nanosheets for high-power sodium-ion hybrid capacitors.* Nature Communications, 2015. **6**: p. 6544.

[45]. Pan, C., et al., *Research on energy management of dual energy storage system based on the simulation of urban driving schedules.* International Journal of Electrical Power & Energy Systems, 2013. **44**(1): p. 37-42.

[46]. Ike, I.S., et al., *RETRACTED: An overview of mathematical modeling of electrochemical supercapacitors/ultracapacitors.* Journal of Power Sources, 2015. **273**: p. 264-277.

[47]. Marts, J.D., *Enhance Physics-Based Reduced-Order models of Non-Faradic Electrical Double-Layer Capacitor Dynamics.*, in *Electrical and Computer Engineering*. 2018, University of Colorado. p. 109.

[48]. Zhang, L., et al., *A review of supercapacitor modeling, estimation, and applications: A control/management perspective.* Renewable and Sustainable Energy Reviews, 2018. **81**: p. 1868-1878.

[49]. Grahame, D.C., *THE ELECTRICAL DOUBLE LAYER AND THE THEORY OF ELECTROCAPILLARITY*. 1946.

[50]. Bockris, J.O.m., et al., *On the structure of charged interfaces.* Proceedings of the Royal Society of London. Series A. Mathematical and Physical Sciences, 1963. **274**(1356): p. 55-79.

[51]. Nelms, R.M., D.R. Cahela, and B.J. Tatarchuk, *Modeling double-layer capacitor behavior using ladder circuits.* IEEE Transactions on Aerospace and Electronic Systems, 2003. **39**(2): p. 430-438.

[52]. Jiya, I.N., N. Gurusinghe, and R. Gouws, *Electrical Circuit Modelling of Double Layer Capacitors for Power Electronics and Energy Storage Applications: A Review*. 2018. **7**(11): p. 268.

[53]. Martín, R., et al., *Modeling of Electrochemical Double Layer Capacitors by Means of Fractional Impedance.* Journal of Computational and Nonlinear Dynamics, 2008. **3**(2).

[54]. Cultura, A.B. and Z.M. Salameh. *Modeling, Evaluation and Simulation of a Supercapacitor Module for Energy Storage Application*. in *International Conference on Computer Information Systems and Industrial Applications*. 2015. Atlantis Press.

[55]. Negroiu, R., et al. *Comparison between Zubieta model of supercapacitors and their real behavior*. in *2016 IEEE 22nd International Symposium for Design and Technology in Electronic Packaging (SIITME)*. 2016.

[56]. Zubieta, L. and R. Bonert, *Characterization of double-layer capacitors for power electronics applications.* IEEE Transactions on Industry Applications, 2000. **36**(1): p. 199-205.

[57]. Faranda, R., M. Gallina, and D.T. Son. *A new simplified model of Double-Layer Capacitors*. in *2007 International Conference on Clean Electrical Power*. 2007.

[58]. Pucci, M., et al. *Parameter identification of a Double-Layer-Capacitor 2-branch model by a least-squares method*. in *IECON 2013 - 39th Annual Conference of the IEEE Industrial Electronics Society*. 2013.

[59]. Kai, W., et al. *A review of modeling research on supercapacitor*. in *2017 Chinese Automation Congress (CAC)*. 2017.

[60]. Pech, D., et al., *Ultrahigh-power micrometre-sized supercapacitors based on onion-like carbon.* Nature Nanotechnology, 2010. **5**: p. 651.

[61]. Lu, W. and L. Dai, *Carbon Nanotube Supercapacitors*. 2010.

[62]. Xiong, G., A. Kundu, and T.S. Fisher, *Thermal Management in Electrochemical Energy Storage Systems*, in *Thermal Effects in Supercapacitors*. 2015, Springer International Publishing: Cham. p. 1-10.

[63]. Hung, K., et al., *Wide-temperature range operation supercapacitors from nanostructured activated carbon fabric.* Journal of Power Sources, 2009. **193**(2): p. 944-949.

[64]. Farhadi, M. and O. Mohammed, *Adaptive Energy Management in Redundant Hybrid DC Microgrid for Pulse Load Mitigation.* IEEE Transactions on Smart Grid, 2015. **6**(1): p. 54-62.

[65]. Farhadi, M. and O.A. Mohammed, *Real-Time Operation and Harmonic Analysis of Isolated and Non-Isolated Hybrid DC Microgrid.* IEEE Transactions on Industry Applications, 2014. **50**(4): p. 2900-2909.

[66]. Ke, Q. and J. Wang, *Graphene-based materials for supercapacitor electrodes – A review*. Journal of Materiomics, 2016. **2**(1): p. 37-54.

[67]. Wang, F., et al., *Latest advances in supercapacitors: from new electrode materials to novel device designs.* Chem Soc Rev, 2017. **46**(22): p. 6816-6854.

[68]. Najib, S. and E. Erdem, *Current progress achieved in novel materials for supercapacitor electrodes: mini review.* Nanoscale Advances, 2019. **1**(8): p. 2817-2827.

[69]. Kumar, K., et al., *Recent Advances in Two-Dimensional Nanomaterials for Supercapacitor Electrode Applications.* ACS Energy Letters, 2018. **3**.

[70]. Raymundo-Piñero, E., et al., *Relationship Between the Nanoporous Texture of Activated Carbons and Their Capacitance Properties in Different Electrolytes.* Carbon, 2006. **44**: p. 2498-2507.

[71]. Simon, P. and Y. Gogotsi, *Materials for electrochemical capacitors.* Nat Mater, 2008. **7**(11): p. 845-54.

[72]. Ashok Kumar, N. and J.-B. Baek, *Electrochemical supercapacitors from conducting polyaniline–graphene platforms.* Chemical Communications, 2014. **50**(48): p. 6298-6308.

[73]. Cheng, Q., et al., *Co(OH)2nanosheet-decorated graphene–CNT composite for supercapacitors of high energy density.* Science and Technology of Advanced Materials, 2014. **15**(1): p. 014206.

[74]. You, B., et al., *Graphene Oxide-Dispersed Pristine CNTs Support for MnO2 Nanorods as High Performance Supercapacitor Electrodes.* 2013. **6**(3): p. 474-480.

[75]. Armand, M. and J.M. Tarascon, *Building better batteries.* Nature, 2008. **451**(7179): p. 652-657.

[76]. Wang, H., et al., *Graphene-nickel cobaltite nanocomposite asymmetrical supercapacitor with commercial level mass loading.* 2012. **5**(9): p. 605-617.

[77]. Jun, B.-M., et al., *Review of MXenes as new nanomaterials for energy storage/delivery and selected environmental applications.* 2019. **12**(3): p. 471-487.

[78]. Kim, H., et al., *Encapsulated, High-Performance, Stretchable Array of Stacked Planar Micro-Supercapacitors as Waterproof Wearable Energy Storage Devices.* ACS Applied Materials & Interfaces, 2016. **8**(25): p. 16016-16025.

[79]. Ye, J., et al., *Direct Laser Writing of Graphene Made from Chemical Vapor Deposition for Flexible, Integratable Micro-Supercapacitors with Ultrahigh Power Output.* 2018. **30**(27): p. 1801384.

[80]. Patil, S.J., J.S. Park, and D.W. Lee. *All Solid-State Flexible Micro-Supercapacitor Based on Hybrid Electrodes for Power Application*. in *2019 IEEE 32nd International Conference on Micro Electro Mechanical Systems (MEMS)*. 2019.

[81]. Beidaghi, M., W. Chen, and C. Wang, *Design, fabrication, and evaluation of on-chip micro-supercapacitors*. SPIE Defense, Security, and Sensing. Vol. 8035. 2011: SPIE.

[82]. Beidaghi, M. and C. Wang, *On-chip micro-power: three-dimensional structures for micro-batteries and micro-supercapacitors*. SPIE Defense, Security, and Sensing. Vol. 7679. 2010: SPIE.

[83]. Pan, Z., et al., *All-Solid-State Fiber Supercapacitors with Ultrahigh Volumetric Energy Density and Outstanding Flexibility.* 2019. **9**(9): p. 1802753.

[84]. Han, Y., et al., *Recent progress in 2D materials for flexible supercapacitors.* Journal of Energy Chemistry, 2018. **27**(1): p. 57-72.

[85]. Zhong, C., et al., *A review of electrolyte materials and compositions for electrochemical supercapacitors.* Chemical Society Reviews, 2015. **44**(21): p. 7484-7539.

[86]. Ghaffarzadeh, K., *Graphene, 2D Materials and Carbon Nanotubes: Markets, Technologies and Opportunities 2019-2029*. 2019.

[87]. Jiang, J., et al., *Highly ordered macroporous woody biochar with ultra-high carbon content as supercapacitor electrodes.* Electrochimica Acta, 2013. **113**: p. 481-489.

[88]. Hall, P.J., et al., *Energy storage in electrochemical capacitors: designing functional materials to improve performance.* Energy & Environmental Science, 2010. **3**(9): p. 1238-1251.

[89]. Berenguer-Murcia, Á., et al., *Binderless thin films of zeolite-templated carbon electrodes useful for electrochemical microcapacitors with ultrahigh rate performance.* Physical Chemistry Chemical Physics, 2013. **15**(25): p. 10331-10334.

[90]. Lukatskaya, M.R., et al., *Cation intercalation and high volumetric capacitance of two-dimensional titanium carbide.* Science, 2013. **341**(6153): p. 1502-5.

[91]. Pei, J., et al., *Producing air-stable monolayers of phosphorene and their defect engineering.* Nat Commun, 2016. **7**: p. 10450.

[92]. Xia, J., et al., *Measurement of the quantum capacitance of graphene.* Nature Nanotechnology, 2009. **4**(8): p. 505-509.

[93]. Stoller, M.D., et al., *Interfacial capacitance of single layer graphene.* Energy & Environmental Science, 2011. **4**(11): p. 4685-4689.

[94]. Kumar, K.S., et al., *Recent Advances in Two-Dimensional Nanomaterials for Supercapacitor Electrode Applications.* ACS Energy Letters, 2018. **3**(2): p. 482-495.

[95]. Kurtoglu, M., et al., *First principles study of two-dimensional early transition metal carbides.* MRS Communications, 2012. **2**(4): p. 133-137.

[96]. Anasori, B., et al., *Two-Dimensional, Ordered, Double Transition Metals Carbides (MXenes).* ACS Nano, 2015. **9**(10): p. 9507-9516.

[97]. Carlsson, J.-O. and P.M. Martin, *Chapter 7 - Chemical Vapor Deposition*, in *Handbook of Deposition Technologies for Films and Coatings (Third Edition)*, P.M. Martin, Editor. 2010, William Andrew Publishing: Boston. p. 314-363.

[98]. Rao, C.N.R., et al., *Graphene: The New Two-Dimensional Nanomaterial.* 2009. **48**(42): p. 7752-7777.

[99]. Mattevi, C., H. Kim, and M. Chhowalla, *A review of chemical vapour deposition of graphene on copper.* Journal of Materials Chemistry, 2011. **21**(10): p. 3324-3334.

[100]. Choi, W., et al., *Synthesis of Graphene and Its Applications: A Review.* Critical Reviews in Solid State and Materials Sciences, 2010. **35**(1): p. 52-71.

[101]. Bae, S., et al., *Roll-to-roll production of 30-inch graphene films for transparent electrodes.* Nature Nanotechnology, 2010. **5**: p. 574.

[102]. Li, X., et al., *Large-Area Synthesis of High-Quality and Uniform Graphene Films on Copper Foils.* 2009. **324**(5932): p. 1312-1314.

[103]. Author: John R. Ferraro, K.N.a.C.W.B., *Chapter 1: Basic Theory*, in *Introductory Raman Spectroscopy*. 2010, Elsevier.

[104]. Ferrari, A.C., et al., *Raman Spectrum of Graphene and Graphene Layers.* Physical Review Letters, 2006. **97**(18): p. 187401.

[105]. Bao, W., et al., *High mobility ambipolar MoS2 field-effect transistors: Substrate and dielectric effects.* 2013. **102**(4): p. 042104.

[106]. Withers, F., et al., *Electron transport of WS2 transistors in a hexagonal boron nitride dielectric environment.* Scientific Reports, 2014. **4**(1): p. 4967.

[107]. Zhong, H., et al., *Interfacial Properties of Monolayer and Bilayer MoS2 Contacts with Metals: Beyond the Energy Band Calculations.* Scientific Reports, 2016. **6**(1): p. 21786.

[108]. M, T. and D.J. Late, *Temperature Dependent Phonon Shifts in Single-Layer WS2.* ACS Applied Materials & Interfaces, 2014. **6**(2): p. 1158-1163.

[109]. Tan, P.-H., *Raman Spectroscopy of Two-Dimensional Materials*, ed. T. Robert Hull, USA, et al. 2019: Springer.

[110]. Malard, L.M., et al., *Raman spectroscopy in graphene.* Physics Reports, 2009. **473**(5): p. 51-87.

[111]. Shearer, C.J., et al., *Accurate thickness measurement of graphene.* Nanotechnology, 2016. **27**(12): p. 125704.

[112]. Ho, J.R.C.a.P., *Introduction to Chemical Vapor Deposition (CVD)*, A. International, Editor. 2001.

[113]. Yuping, S., et al., *Na-assisted fast growth of large single-crystal MoS 2 on sapphire.* Nanotechnology, 2019. **30**(3): p. 034002.

[114]. Yongji, G., et al., *Direct growth of MoS 2 single crystals on polyimide substrates.* 2D Materials, 2017. **4**(2): p. 021028.

[115]. Dumcenco, D., et al., *Large-Area Epitaxial Monolayer MoS2.* ACS Nano, 2015. **9**(4): p. 4611-4620.

[116]. Li, M.-Y., et al., *Epitaxial growth of a monolayer WSe<sub>2</sub>-MoS<sub>2</sub> lateral p-n junction with an atomically sharp interface.* 2015. **349**(6247): p. 524-528.

[117]. Chen, J., et al., *Chemical Vapor Deposition of Large-Size Monolayer MoSe2 Crystals on Molten Glass.* Journal of the American Chemical Society, 2017. **139**(3): p. 1073-1076.

[118]. Yang, P., et al., *Batch production of 6-inch uniform monolayer molybdenum disulfide catalyzed by sodium in glass.* Nature Communications, 2018. **9**(1): p. 979.

[119]. Barreau, N. and J.C. Bernède, *Low-temperature preparation of MoS 2 thin films on glass substrate with NaF additive*. Vol. 403. 2002. 505-509.

[120]. Braunger, D., et al., *Influence of sodium on the growth of polycrystalline Cu(In,Ga)Se2 thin films.* Thin Solid Films, 2000. **361-362**: p. 161-166.

[121]. Şar, H., et al., *Long-Term Stability Control of CVD-Grown Monolayer MoS2.* 2019. **13**(7): p. 1800687.

[122]. Lee, C., et al., *Anomalous Lattice Vibrations of Single- and Few-Layer MoS2.* ACS Nano, 2010. **4**(5): p. 2695-2700.

[123]. Li, H., et al., *From Bulk to Monolayer MoS2: Evolution of Raman Scattering.* 2012. **22**(7): p. 1385-1390.

[124]. Mak, K.F., et al., *Tightly bound trions in monolayer MoS2.* Nature Materials, 2013. **12**(3): p. 207-211.

[125]. Lin, Y., et al., *Dielectric Screening of Excitons and Trions in Single-Layer MoS2.* Nano Letters, 2014. **14**(10): p. 5569-5576.

[126]. Xie, Y., et al., *Controllable growth of monolayer MoS2by chemical vapor deposition via close MoO2precursor for electrical and optical applications.* Nanotechnology, 2017. **28**(8): p. 084001.

[127]. Lanzillo, N., et al., *Temperature-dependent Phonon Shifts in Monolayer MoS2.* Applied Physics Letters, 2013. **103**.

[128]. Eftekhari, A., *Molybdenum diselenide (MoSe2) for energy storage, catalysis, and optoelectronics.* Applied Materials Today, 2017. **8**: p. 1-17.

[129]. Yang, C.-P., Y.-X. Yin, and Y.-G. Guo, *Elemental Selenium for Electrochemical Energy Storage.* The Journal of Physical Chemistry Letters, 2015. **6**(2): p. 256-266.

[130]. Ma, H., et al., *Thickness-Tunable Synthesis of Ultrathin Type-II Dirac Semimetal PtTe2 Single Crystals and Their Thickness-Dependent Electronic Properties.* Nano Letters, 2018. **18**(6): p. 3523-3529.

[131]. Jadczak, J., et al., *Composition dependent lattice dynamics in MoSxSe(2–x) alloys.* 2014. **116**(19): p. 193505.

[132]. WILLIAMS, J.P., F.J. FARNCOMB, and T.S. MAGLIOCCA, *Determination of Sulfur in Glass.* 1957. **40**(10): p. 352-354.

[133]. Tonndorf, P., et al., *Photoluminescence emission and Raman response of monolayer MoS2, MoSe2, and WSe2.* Optics Express, 2013. **21**(4): p. 4908-4916.

[134]. Zuxin, C., et al., *Wafer-Size and Single-Crystal MoSe_2 Atomically Thin Films Grown on GaN Substrate for Light Emission and Harvesting.* ACS Applied Materials & Interfaces, 2016. **8**.

[135]. Wang, X., et al., *Chemical Vapor Deposition Growth of Crystalline Monolayer MoSe2.* ACS Nano, 2014. **8**(5): p. 5125-5131.

[136]. Shaw, J.C., et al., *Chemical vapor deposition growth of monolayer MoSe2 nanosheets.* 2014. **7**(4): p. 511-517.

[137]. Naguib, M., et al., *Two-Dimensional Nanocrystals Produced by Exfoliation of Ti3AlC2.* 2011. **23**(37): p. 4248-4253.

[138]. Ghidiu, M., et al., *Synthesis and characterization of two-dimensional Nb4C3 (MXene).* Chemical Communications, 2014. **50**(67): p. 9517-9520.

[139]. Naguib, M., et al., *New Two-Dimensional Niobium and Vanadium Carbides as Promising Materials for Li-Ion Batteries.* Journal of the American Chemical Society, 2013. **135**(43): p. 15966-15969.

[140]. Naguib, M., et al., *Two-Dimensional Transition Metal Carbides.* ACS Nano, 2012. **6**(2): p. 1322-1331.

[141]. Halim, J., et al., *Transparent Conductive Two-Dimensional Titanium Carbide Epitaxial Thin Films.* Chemistry of Materials, 2014. **26**(7): p. 2374-2381.

[142]. Ghidiu, M., et al., *Conductive two-dimensional titanium carbide 'clay' with high volumetric capacitance.* Nature, 2014. **516**(7529): p. 78-81.

[143]. Halim, J., et al., *Synthesis and Characterization of 2D Molybdenum Carbide (MXene).* 2016. **26**(18): p. 3118-3127.

[144]. Xu, C., et al., *Large-area high-quality 2D ultrathin Mo2C superconducting crystals.* Nature Materials, 2015. **14**(11): p. 1135-1141.

[145]. Mildred S. Dresselhaus, G.D., Ado Jorio, *Group Theory: Application to the Physics of Condensed Matter*. 2010: Springer, Year: 2008.

[146]. Li, T., et al., *Probing the Domain Architecture in 2D α-Mo2C via Polarized Raman Spectroscopy.* 2019. **31**(8): p. 1807160.

[147]. Novoselov, K.S., et al., *Electric Field Effect in Atomically Thin Carbon Films.* 2004. **306**(5696): p. 666-669.

[148]. Bolotin, K.I., et al., *Ultrahigh electron mobility in suspended graphene.* Solid State Communications, 2008. **146**(9): p. 351-355.

[149]. Lee, C., et al., *Measurement of the Elastic Properties and Intrinsic Strength of Monolayer Graphene.* 2008. **321**(5887): p. 385-388.

[150]. Lemine, A.S., et al., *Graphene a promising electrode material for supercapacitors—A review.* 2018. **42**(14): p. 4284-4300.

[151]. Zang, X., et al., *Evaluation of layer-by-layer graphene structures as supercapacitor electrode materials.* 2014. **115**(2): p. 024305.

[152]. Vivekchand, S.R.C., et al., *Graphene-based electrochemical supercapacitors.* 2008. **120**(1): p. 9-13.

[153]. Si, Y. and E.T. Samulski, *Exfoliated Graphene Separated by Platinum Nanoparticles.* Chemistry of Materials, 2008. **20**(21): p. 6792-6797.

[154]. Qiu, L., et al., *Dispersing Carbon Nanotubes with Graphene Oxide in Water and Synergistic Effects between Graphene Derivatives.* 2010. **16**(35): p. 10653-10658.

[155]. Wang, G., et al., *Flexible Pillared Graphene-Paper Electrodes for High-Performance Electrochemical Supercapacitors.* 2012. **8**(3): p. 452-459.

[156]. Zhang, L.L., R. Zhou, and X.S. Zhao, *Graphene-based materials as supercapacitor electrodes.* Journal of Materials Chemistry, 2010. **20**(29): p. 5983-5992.

[157]. Stoller, M.D., et al., *Graphene-Based Ultracapacitors.* Nano Letters, 2008. **8**(10): p. 3498-3502.

[158]. Kim, S.J., et al., *Ultraclean Patterned Transfer of Single-Layer Graphene by Recyclable Pressure Sensitive Adhesive Films.* Nano Letters, 2015. **15**(5): p. 3236-3240.

[159]. Suk, J.W., et al., *Transfer of CVD-Grown Monolayer Graphene onto Arbitrary Substrates.* ACS Nano, 2011. **5**(9): p. 6916-6924.

[160]. Allagui, A., et al., *Reevaluation of Performance of Electric Double-layer Capacitors from Constant-current Charge/Discharge and Cyclic Voltammetry.* Scientific Reports, 2016. **6**: p. 38568.

[161]. Stoller, M. and R. Ruoff, *Review of Best Practice Methods for Determining an Electrode Material's Performance for Ultracapacitors.* Energy & Environmental Science, 2010. **3**.

[162]. Stoller, M.D. and R.S. Ruoff, *Best practice methods for determining an electrode material's performance for ultracapacitors.* Energy & Environmental Science, 2010. **3**(9): p. 1294-1301.

[163]. Choi, W., et al., *Recent development of two-dimensional transition metal dichalcogenides and their applications.* Materials Today, 2017. **20**(3): p. 116-130.

[164]. Yang, Y., et al., *Edge-Oriented MoS2 Nanoporous Films as Flexible Electrodes for Hydrogen Evolution Reactions and Supercapacitor Devices.* 2014. **26**(48): p. 8163-8168.

[165]. Choudhary, N., et al., *High-Performance One-Body Core/Shell Nanowire Supercapacitor Enabled by Conformal Growth of Capacitive 2D WS2 Layers.* ACS Nano, 2016. **10**(12): p. 10726-10735.

[166]. Acerce, M., D. Voiry, and M. Chhowalla, *Metallic 1T phase MoS2 nanosheets as supercapacitor electrode materials.* Nature Nanotechnology, 2015. **10**: p. 313.

[167]. Becerril, H.A., et al., *Evaluation of solution-processed reduced graphene oxide films as transparent conductors.* ACS Nano, 2008. **2**(3): p. 463-70.

[168]. Gunes, F., et al., *Layer-by-layer doping of few-layer graphene film.* ACS Nano, 2010. **4**(8): p. 4595-600.

[169]. Gan, S., et al., *Spontaneous and Fast Growth of Large-Area Graphene Nanofilms Facilitated by Oil/Water Interfaces.* 2012. **24**(29): p. 3958-3964.

[170]. Li, D., et al., *Processable aqueous dispersions of graphene nanosheets.* Nat Nanotechnol, 2008. **3**(2): p. 101-5.

[171]. Wu, Q., et al., *Supercapacitors Based on Flexible Graphene/Polyaniline Nanofiber Composite Films.* ACS Nano, 2010. **4**(4): p. 1963-1970.

[172]. Zhang, K., et al., *Graphene/Polyaniline Nanofiber Composites as Supercapacitor Electrodes.* Chemistry of Materials - CHEM MATER, 2010. **22**.

# Appendix

## Capacitance calculation data

| Active Material | SR (mV/s) | CV Area | V2 | v1 | c(F) | c(uF) | EA | SpC (uF/cm2) | Volume | VC F/cm3 | Density | GC (F/g) |
|---|---|---|---|---|---|---|---|---|---|---|---|---|
| 1 Layer graphene | 1 | 5.32E-08 | 0.766407 | 0.0670486 | 3.80E-05 | 38.003834 | 3.46 | 43.93506814 | 2.1798E-07 | 697.382034 | 2.267 | 307.62331 |
| | 2 | 5.18E-08 | 0.7526581 | 0.0388634 | 1.81E-05 | 18.141596 | 3.46 | 20.97294371 | 2.1798E-07 | 332.9038684 | 2.267 | 146.84776 |
| | 5 | 8.44E-08 | 0.7139322 | 0.0317599 | 1.24E-05 | 12.378295 | 3.46 | 14.31016728 | 2.1798E-07 | 227.1455124 | 2.267 | 100.19652 |
| | 10 | 1.24E-07 | 0.6754354 | 0.0432172 | 9.80E-06 | 9.7985957 | 3.46 | 11.32785624 | 2.1798E-07 | 179.807242 | 2.267 | 79.31506 |
| | 20 | 2.03E-07 | 0.6891842 | 0.0418423 | 7.84E-06 | 7.8436142 | 3.46 | 9.067762034 | 2.1798E-07 | 143.9327307 | 2.267 | 63.490397 |
| | 50 | 3.70E-07 | 0.6614574 | 0.0617782 | 6.18E-06 | 6.1769193 | 3.46 | 7.140947199 | 2.1798E-07 | 113.3483682 | 2.267 | 49.99928 |
| | 100 | 6.70E-07 | 0.7132447 | 0.0466544 | 5.02E-06 | 5.0242406 | 3.46 | 5.808370689 | 2.1798E-07 | 92.19636015 | 2.267 | 40.668884 |
| | 150 | 9.30E-07 | 0.747846 | 0.0519248 | 4.45E-06 | 4.4539 | 3.46 | 5.149017374 | 2.1798E-07 | 81.73043451 | 2.267 | 36.052243 |
| | 200 | 9.72E-07 | 0.6525206 | 0.0840055 | 4.28E-06 | 4.2760384 | 3.46 | 4.943396994 | 2.1798E-07 | 78.46661895 | 2.267 | 34.612536 |
| | 500 | 2.04E-06 | 0.665582 | 0.066132 | 3.40E-06 | 3.402452 | 3.46 | 3.933470506 | 2.1798E-07 | 62.43603978 | 2.267 | 27.541261 |
| | | | | | | | | | | | | |
| 2 Layer graphene | 1 | 7.93E-08 | 0.7875855 | 0.5080156 | 1.42E-04 | 141.89582 | 4.5 | 126.1296205 | 5.67E-07 | 1001.028734 | 2.267 | 441.56539 |
| | 2 | 2.02E-07 | 0.7939394 | 0.0026393 | 6.37E-05 | 63.671482 | 4.5 | 56.59687297 | 5.67E-07 | 449.1815315 | 2.267 | 198.13918 |
| | 5 | 3.36E-07 | 0.7983382 | 0.001173 | 4.22E-05 | 42.191129 | 4.5 | 37.503226 | 5.67E-07 | 297.6446508 | 2.267 | 131.29451 |
| | 10 | 5.17E-07 | 0.7973607 | 0.0050831 | 3.26E-05 | 32.601893 | 4.5 | 28.97946042 | 5.67E-07 | 229.9957176 | 2.267 | 101.45378 |
| | 20 | 8.28E-07 | 0.800782 | 0.0036168 | 2.60E-05 | 25.965164 | 4.5 | 23.0801456 | 5.67E-07 | 183.1757587 | 2.267 | 80.800952 |
| | 50 | 1.57E-06 | 0.7998045 | 0.0026393 | 1.97E-05 | 19.695792 | 4.5 | 17.50737069 | 5.67E-07 | 138.9473865 | 2.267 | 61.291304 |
| | 100 | 2.47E-06 | 0.7958944 | 0.0060606 | 1.57E-05 | 15.656205 | 4.5 | 13.9166264 | 5.67E-07 | 110.4494159 | 2.267 | 48.720519 |
| | 150 | 3.18E-06 | 0.7998045 | 0.0060606 | 1.34E-05 | 13.363042 | 4.5 | 11.87825999 | 5.67E-07 | 94.27190468 | 2.267 | 41.584431 |
| | 200 | 3.80E-06 | 0.7998045 | 0.0045943 | 1.20E-05 | 11.955173 | 4.5 | 10.62682032 | 5.67E-07 | 84.33984384 | 2.267 | 37.203284 |
| | 500 | 6.97E-06 | 0.7998045 | 0.001173 | 8.72E-06 | 8.7223334 | 4.5 | 7.753185247 | 5.67E-07 | 61.53321624 | 2.267 | 27.143016 |
| | | | | | | | | | | | | |
| 4 Layer graphene | 1 | 2.85E-07 | 0.7993157 | 0.0085044 | 1.80E-04 | 180.17445 | 4.5 | 160.1550688 | 1.13E-06 | 635.5359873 | 2.267 | 280.3423 |
| | 2 | 3.11E-07 | 0.7993157 | 0.0041056 | 9.77E-05 | 97.658145 | 4.5 | 86.80724032 | 1.13E-06 | 344.4731759 | 2.267 | 151.95111 |
| | 5 | 4.84E-07 | 0.800782 | 0.001173 | 6.05E-05 | 60.543466 | 4.5 | 53.81641434 | 1.13E-06 | 213.5571998 | 2.267 | 94.202558 |
| | 10 | 7.07E-07 | 0.7993157 | 0.0026393 | 4.44E-05 | 44.389602 | 4.5 | 39.4574238 | 1.13E-06 | 156.5770786 | 2.267 | 69.067966 |
| | 20 | 1.09E-06 | 0.7993157 | 0.0055718 | 3.42E-05 | 34.194279 | 4.5 | 30.39491461 | 1.13E-06 | 120.6147405 | 2.267 | 53.204561 |
| | 50 | 2.00E-06 | 0.7993157 | 0.0026393 | 2.51E-05 | 25.131031 | 4.5 | 22.33869382 | 1.13E-06 | 88.64561041 | 2.267 | 39.102607 |
| | 100 | 3.12E-06 | 0.8017595 | 0.0026393 | 1.95E-05 | 19.490434 | 4.5 | 17.32483001 | 1.13E-06 | 68.74932544 | 2.267 | 30.326125 |
| | 150 | 3.99E-06 | 0.7993157 | 0.0070381 | 1.68E-05 | 16.794786 | 4.5 | 14.92869905 | 1.13E-06 | 59.24086924 | 2.267 | 26.131835 |
| | 200 | 4.77E-06 | 0.7978495 | 0.0070381 | 1.51E-05 | 15.079355 | 4.5 | 13.4038712 | 1.13E-06 | 53.18996508 | 2.267 | 23.462711 |
| | 500 | 8.93E-06 | 0.7978495 | 0.001173 | 1.12E-05 | 11.204549 | 4.5 | 9.959598855 | 1.13E-06 | 39.52221768 | 2.267 | 17.433709 |
| | | | | | | | | | | | | |
| 8 Layer graphene | 1 | 6.18E-07 | 0.7972671 | -0.098924 | 3.45E-04 | 344.86953 | 4.5 | 306.550693 | 2.27E-06 | 608.235502 | 2.267 | 268.29974 |
| | 2 | 4.35E-07 | 0.7986873 | -0.0802238 | 1.24E-04 | 123.78954 | 4.5 | 110.0351427 | 2.27E-06 | 218.3236958 | 2.267 | 96.305115 |
| | 5 | 3.88E-07 | 0.8018391 | -0.0845977 | 4.38E-05 | 43.824107 | 4.5 | 38.95476141 | 2.27E-06 | 77.29119328 | 2.267 | 34.094042 |
| | 10 | 4.48E-07 | 0.8004598 | -0.085977 | 2.53E-05 | 25.28319 | 4.5 | 22.4739471 | 2.27E-06 | 44.59116487 | 2.267 | 19.66968 |
| | 20 | 6.18E-07 | 0.8004598 | -0.0832184 | 1.75E-05 | 17.490842 | 4.5 | 15.54741502 | 2.27E-06 | 30.84804567 | 2.267 | 13.607431 |
| | 50 | 9.93E-07 | 0.7993103 | -0.082069 | 1.13E-05 | 11.262608 | 4.5 | 10.01120744 | 2.27E-06 | 19.86350683 | 2.267 | 8.7620233 |
| | 100 | 1.38E-06 | 0.797931 | -0.0806897 | 7.84E-06 | 7.8383654 | 4.5 | 6.967435897 | 2.27E-06 | 13.82427757 | 2.267 | 6.0980492 |
| | 150 | 1.63E-06 | 0.7993103 | -0.082069 | 6.18E-06 | 6.181561 | 4.5 | 5.494720918 | 2.27E-06 | 10.90222404 | 2.267 | 4.8090975 |
| | 200 | 1.83E-06 | 0.8018391 | -0.0832184 | 5.17E-06 | 5.1678847 | 4.5 | 4.593675325 | 2.27E-06 | 9.114435168 | 2.267 | 4.0204831 |
| | | | | | | | | | | | | |
| Mxene Graphene | 1 | 9.13E-07 | 0.7396872 | 0.1355816 | 7.55E-04 | 755.31334 | 4.5 | 671.3896397 | | | | |
| | 2 | 6.02E-07 | 0.7323558 | 0.0280547 | 2.14E-04 | 213.76156 | 4.5 | 190.0102799 | | | | |
| | 5 | 8.20E-07 | 0.7005865 | 0.0231672 | 1.21E-04 | 121.02415 | 4.5 | 107.5770201 | | | | |
| | 10 | 1.12E-06 | 0.6981427 | 0.0480938 | 8.65E-05 | 86.491189 | 4.5 | 76.88105664 | | | | |
| | 20 | 1.76E-06 | 0.6956989 | 0.0466276 | 6.78E-05 | 67.770284 | 4.5 | 60.24025201 | | | | |
| | 50 | 3.25E-06 | 0.6790811 | 0.0495601 | 5.16E-05 | 51.565872 | 4.5 | 45.83633043 | | | | |
| | 100 | 5.01E-06 | 0.6688172 | 0.0627566 | 4.13E-05 | 41.339265 | 4.5 | 36.74601333 | | | | |
| | 150 | 6.09E-06 | 0.6253177 | 0.0647116 | 3.62E-05 | 36.236854 | 4.5 | 32.21053694 | | | | |
| | 200 | 8.02E-06 | 0.6937439 | 0.0744868 | 3.24E-05 | 32.389173 | 4.5 | 28.79037611 | | | | |
| | 500 | 1.46E-05 | 0.6785924 | 0.0896383 | 2.48E-05 | 24.772391 | 4.5 | 22.01990285 | | | | |

**Key**

| | |
|---|---|
| CV area | Area under the CV curve |
| C | Capacitance of a single electrode, |
| EA | Total area of the two electrodes |
| SpC | Specific capacitance |

| | |
|---|---|
| VC | Volumetric capacitance |
| GC | Gravimetric capacitance. |

# Ibrahim Wonge Lisheshar

Sütlüce M. Kaddilli sk: 04, 02, Eskişehir (Turkey)

+905392068178

ibn.lisha@yahoo.com, wli562@eskisehir.edu.tr

https://www.linkedin.com/in/ibrahim-lisheshar-b7869641/


## Research Interests

2D materials, their electronic and energy storage applications.

## Work Experience

*Sep-2015 to Jul-2016*

### Higher education teaching professional

MCD Bilingual High School, Yaounde (Cameroon)

Guiding students to an understanding of Mathematical equations and their application to problem solving.

Helping to culture into students, rapid problem solving, thinking and analytical skills.

## Education and Training

*Sep-2017 to Present*

### Masters of Science in Electronics Engineering

EQF level 7

Eskisehir Technical University (Previously part of the University of Anatolya), Eskisehir (Turkey)

- EEM552 Micro-Nanodevices and Thin Film Applications
- ITN522 Introduction to Micro and Nano Fabrication
- EEM547 Fundamentals of Detection and Estimation
- EEM507 Integrated Optical Waveguides

## Projects Realized

### Growth Of Transition Metal Dichalcogenites.

- $MoS_2$ (765µm), Fabrication of $MoS_2$ phototransistor
- $MoSe_2$, Fabrication of $MoSe_2$ phototransistors

## Personal Skills

### Languages

- English – Toefl Score: 98
- French
- Turkish – C1 Certificate

## Communication Skills

Good communication skills gained through living and studying in a multicultural environment as well as through teaching

## Job related Skills

Monitoring Skills - As a teacher I was able to assess the weaknesses of students, developing ways to ameliorate them, while observing their individual growth.

*Lab Related Skills*

Chemical Vapor Deposition

- Growth of TMDC ($MoS_2$/$MoSe_2$)
- Growth of Graphene

Photolithography

- Fabrication of transistors
- Hall Sensors

Characerization Tools

- Raman/ PL
- Atomic Force Microscopy
- Four point probe characterization

## Digital Skills

*Programing Languages*

- Java SE/C++ (Self taught)
- HTML, CSS, JS and Node JS. (Online course)

*Simulation*

- Matlab, Matlab Simulink.

## Hobies

- Web programing
- Basketball
- Guitar